Ultrasonic velocities, densities, viscosities, electrical conductivities, Raman spectra, and molecular dynamics simulations of aqueous solutions of $Mg(OAc)_2$ and $Mg(NO_3)_2$: Hofmeister effects and ion pair formation

Abdul Wahab[a], Sekh Mahiuddin[a*], Glenn Hefter[b*], Werner Kunz[c*], Babak Minofar[d], and Pavel Jungwirth[d*]

[a]Material Science Division, Regional Research Laboratory, Jorhat - 785 006, Assam, India
[b]Department of Chemistry, Murdoch University, Murdoch WA 6150, Australia
[c]Institut für Physikalische und Theoretische Chemie, Universität Regensburg, D-93040 Regensburg, Germany
[d]Institute of Organic Chemistry and Biochemistry, Academy of Sciences of the Czech Republic, and Center for Biomolecules and Complex Molecular Systems, Flemingovo nám. 2, 16610 Prague 6, Czech Republic

Abstract

The ultrasonic velocities, densities, viscosities, and electrical conductivities of aqueous solutions of magnesium nitrate and magnesium acetate have been measured from dilute to saturation concentrations at $0 \leq t/°C \leq 50$. The temperature derivative of the isentropic compressibility, κ_s, became zero at 2.28 mol kg^{-1} and 2.90 mol kg^{-1} for $Mg(OAc)_2$ and $Mg(NO_3)_2$ solutions, respectively, at 25 °C. The total hydration numbers of the dissolved ions were estimated to be, respectively, 24.3 and 19.2 at these concentrations. Differences in κ_s for various M^{2+} salts, using the present and literature data, correlated with reported M^{2+}–OH_2 bond lengths and to a lesser extent with cationic charge density (ionic radius). The influence of anions on κ_s appears to follow the Hofmeister series and also correlates approximately with the anionic charge density. Substantial differences between $Mg(OAc)_2$(aq) and $Mg(NO_3)_2$(aq) occur with respect to their structural relaxation times (derived from compressibility and viscosity data) and their electrical conductivities. These differences were attributed to much greater ion association in $Mg(OAc)_2$ solutions. Raman spectra recorded at 28 °C confirmed the presence of various types of contact ion pairs including mono- and bidentate complexes in $Mg(OAc)_2$(aq). In $Mg(NO_3)_2$(aq) only non-contact ion pairs appear to be formed even at high concentrations. The experimental results are supported by molecular dynamics simulations, which also reveal the much stronger tendency of OAc^-

compared to NO_3^- to associate with Mg^{2+} in aqueous solutions. The simulations also allow an evaluation of the ion-ion and ion-water radial distribution functions and cumulative sums, and provide a molecular picture of ion hydration in $Mg(OAc)_2$(aq) and $Mg(NO_3)_2$(aq) at varying concentrations.

Keywords: Hofmeister effects, ion pairs, isentropic compressibity, magnesium acetate, magnesium nitrate, molecular dynamics, Raman spectra

*Corresponding authors: mahirrljt@yahoo.com (Sekh Mahiuddin); g.hefter@murdoch.edu.au (Glenn Hefter); werner.kunz@chemie.uni-regensburg.de (Werner Kunz); pavel.jungwirth@uochb.cas.cz (Pavel Jungwirth)

1. Introduction

The presence, nature and concentration of salts can dramatically alter the solubility and behaviour of other molecules in solution.[1] Consequently, the solvation of ions in aqueous media is of prime importance in many areas including surface chemistry, environmental chemistry and geochemistry. In particular, to understand the processes occurring in living cells[2,3] (such as ion transport across cell membranes, the functioning of proteins and ion channels) the nature of ion hydration is prerequisite information. The hydration of multivalent metal ions is especially interesting because of the presence of well-defined solvation shells and the formation of specific complexes.[4] Magnesium ion is present at moderate concentrations in living cells[5] and sea water[6] and its salts are important industrially. The acetate ion occurs widely in nature, being produced by microorganisms and by the decomposition of humic acids,[7,8] whilst nitrate is of special environmental importance in the atmosphere and in soils.[9]

It is well established[10–16] that six water molecules are strongly bound in the primary hydration shell of Mg^{2+} in aqueous solutions. In fact, Mg^{2+} retains the hexahydrate structure, with an almost constant Mg^{2+}–$(OH_2)_6$ bond length irrespective of the nature of the counteranion.[12,13] On the basis of X-ray diffraction studies of $Mg(NO_3)_2$(aq), Caminiti et al.,[12] suggested that nitrate ions do not produce any pronounced structuring effect in their neighbourhood. As well as confirming that Mg^{2+} has an inner hydration shell of six they also proposed a second coordination shell of twelve water molecules, which was also suggested by Bol et al.[10] Conductivity[17] and vapour pressure[18] measurements imply that complex formation between Mg^{2+} and NO_3^- in aqueous solutions (at concentrations $m \leq 2.2$ mol kg^{-1}) is unlikely.

Consistent with these measurements, several Raman spectral studies[19–24] have concluded that contact ion pairs do not form in $Mg(NO_3)_2$(aq) up to saturation (3.85 mol dm^{-3}) at 25 ^{o}C. Nevertheless, principal component analysis[25] of Raman spectra has revealed the presence of some associated species at $M \geq 2.5$ mol dm^{-3}, which were earlier assigned to be solvent–shared ion pairs by Chang and Irish.[22] James and Frost[26]

reported the existence of solvent-shared ion pairs in this system even at ≥ 0.5 mol dm^{-3} using a similar approach.

At higher temperatures (up to 120 °C) Peleg[21] showed, again via Raman spectroscopy, that $Mg(OH_2)_6^{2+}$ remained intact, as suggested by Angell,[27] at concentrations ≤ 9.25 mol kg^{-1} but beyond that, NO_3^- entered the primary hydration shell of Mg^{2+}. Peleg also reported the existence of a perturbed quasi-lattice structure for Mg^{2+}–NO_3^- contact ion pairs in $Mg(NO_3)_2{\cdot}2.4H_2O$ and $Mg(NO_3)_2{\cdot}2H_2O$ melts. Irish et al.[28] proposed the presence of two bidentate contact ion pairs: $[Mg^{2+}(H_2O)_4(NO_3^-)]$ and $[Mg^{2+}(H_2O)_2(NO_3^-)_2]$ in $Mg(NO_3)_2{\cdot}2.2H_2O$ melts. Chang and Irish[22] later identified contact ion pairs in 9.25 mol kg^{-1} $Mg(NO_3)_2{\cdot}6H_2O$ and inferred that a monodentate to bidentate conversion occurs as water is further removed. Very recently, Zhang et al.,[23] studied aqueous $Mg(NO_3)_2$ droplets using an electrodynamic balance in conjunction with the Raman spectroscopy and observed a large number of contact ion pairs including monodentate and bidentate species.

Aqueous solutions of $Mg(OAc)_2$ appear particularly interesting with respect to the formation of different types of species at different concentrations. Caminiti et al.[29] reported the presence of a monoacetato complex in 0.25–1.5 mol dm^{-3} aqueous $Mg(OAc)_2$ solutions, employing X-ray scattering and ^{13}C NMR spectroscopy. Conductivity studies in very dilute solutions (≤ 0.002 mol dm^{-3}) indicate ion association in $Mg(OAc)_2$(aq) with a modest association constant, K_A^o, for 1:1 stoichiometry, of ≈ 50 dm^3 mol^{-1}.[30] However, an ultrasonic absorption study[31] suggested that OAc^- did not penetrate into the primary hydration shell of Mg^{2+}.

Investigating the symmetric and antisymmetric stretching modes of the carboxylate group by ATR-IR spectroscopy, Tackett[32] observed only free ions in dilute (0.6 mol dm^{-3}) $Mg(OAc)_2$(aq). Semmler et al.[8] studied the C–C stretching modes in the Raman spectra of OAc^- at a pressure of 9 MPa and temperatures up to 150 °C in solutions containing $MgCl_2$, $Mg(OAc)_2$, NaOAc, and $NaNO_3$ having total mole ratios of OAc^- to Mg^{2+} of 0.5 to 6 and suggested the existence of two monodentate complexes. Nickolov et al.[33] reported the existence of mono– and bisacetato complexes in 0.65–3.24 mol

dm^{-3} $Mg(OAc)_2$ solutions from Raman measurements. Using ATR-IR and Raman spectra of dilute (0.05–0.6 mol dm^{-3}) $Mg(OAc)_2$, Quilès and Burneau[34] found no contact ion pairs, consistent with Tackett.[32] Very recently, Wang et al.[35] studied supersaturated $Mg(OAc)_2$(aq) droplets ($m \geq 3.58$ mol kg^{-1}) using a single-particle levitation technique with in-situ Raman spectroscopy. They detected bidentate complexes and also proposed the formation of bridged bidentate complexes. For a better overview the various species reported in aqueous solutions of $Mg(NO_3)_2$ and $Mg(OAc)_2$ are summarized in Table 1.

Table 1. Different ionic species present in salt solutions obtained from Raman spectra (R), IR spectra (IR), NMR spectra (NMR), X-ray diffraction (X), conductivity (C), vapour pressure (V), hygroscopicity (H) and ultrasonic absorption (UA) methods at ambient temperatures

Solute	Concentration	Ionic species	Method	Ref.
$Mg(NO_3)_2$	1.0, 2.0, 4.0 M	no complexes detected	X	10,12
	very dilute	little association	C	17
	≤ 2.197 *m*	little association	V	18
	2.77–9.25 *m*	solvent-shared ion pairs	R	21
	≥ 9.25 *m*	contact ion pairs[A]	R	21
	2.8–4.9 *m*	solvent-shared ion pairs	R	22
	≥ 9.25 *m*	mono- and bidentate complexes[B]	R	22
	6–2.0 WSR	mono- and bidentate complexes	R & H	23
	2.2 WSR	bidentate complexes[C]	R	28
	≥ 2.5 M	associated species	R	25
	0.5–3.0 M	solvent-shared ion pairs	R	26
$Mg(OAc)_2$	0.05–0.6 M	no complexes detected	IR & R	34
	0.6 M	no complexes detected	IR	32
	≤ 0.002 M	1:1 complex	C	30
	0.65–3.24 M	mono- and bisacetato complexes	R	33
	0.501–5.98 MR	monodentate complexes	R	8
	0.25–1.5 M	monodentate complex	X & NMR	29
	≤ 0.4 M	no contact ion pairs	UA	31
	15.5–2.58 WSR	mono- and bidentate complexes	R & H	35

m = mol kg^{-1}; M = mol dm^{-3}; WSR = water to solute ratio; MR= OAc^- to Mg^{2+} molar ratio; [A]≤120 °C; [B]150–200 °C; [C]>100 °C

Solutions of acetate and nitrate salts at moderate concentrations are also of interest in connection with the ubiquitous, but largely unexplained, Hofmeister series. This series of ions, established originally on the basis of their effects on protein solubilities[36]

has been observed in an impressive range of biological and biochemical phenomena.[37] However, despite some recent progress[38] understanding of this series remains obscure and few papers deal with other than monovalent ions. Since OAc^- and NO_3^- lie towards the two extremes of the Hofmeister series (salting-out and salting-in, respectively) it is of interest to compare their physicochemical properties, which may shed light on this important topic.

This paper, therefore, presents a detailed study of the ultrasonic velocities, densities, viscosities, and electrical conductivities of aqueous solutions of $Mg(NO_3)_2$ and $Mg(OAc)_2$ from dilute to saturation concentrations and as a function of temperature. FT-Raman spectra of these solutions have also been recorded to clarify the role of ion association. The experimental data are complemented by molecular dynamics simulations of aqueous solutions of $Mg(NO_3)_2$ and $Mg(OAc)_2$ at 0.25 and 1 M concentrations. These calculations, which employ periodic boundary conditions to simulate the aqueous bulk, provide a picture with atomic resolution of solvation of individual ions and allow quantification of the degree of ion pairing in the magnesium nitrate vs. acetate solutions in terms of ion–ion pair distribution functions.

2. Experimental

$Mg(OAc)_2{\cdot}4H_2O$ (>99%, SRL, India) and $Mg(NO_3)_2{\cdot}6H_2O$ (>99%, SD Fine Chemicals, India) were recrystallized twice from double–distilled water and then kept in a vacuum desiccator over P_2O_5. All solutions were prepared using double–distilled water and by successive dilution of a stock solution. The concentrations were finally checked by complexometric titration against EDTA.[39] The overall accuracy in the solution preparation was within ±0.3%.

The detailed measurement procedures for ultrasonic velocities at 3 MHz, densities and viscosities are described elsewhere.[40–42] The uncertainties in the measurements of ultrasonic velocity, density and viscosity were within ±0.01%, ±0.01% and ±0.5%, respectively. Electrical conductivities were measured using platinised platinum electrodes and a Precision Component Analyser 6440A (Wayne Kerr, U. K.) at a field

frequency of 1 kHz. The cell constant of 1.237 cm^{-1} was determined by using a 0.1 mol kg^{-1} aqueous KCl solution at different temperatures. The experimental uncertainty in the conductivity values was less than ±0.4%.

Electrical conductivities, ultrasonic velocities and viscosities of both systems were measured from 0 to 50 ^{o}C at 5 ^{o}C intervals as functions of salt concentration ($0.0145 \leq m/\text{mol kg}^{-1} \leq 6.545$). Schott–Geräte CT 1450 or Julabo F32 HP thermostats were used to control solution temperatures to within ±0.02 ^{o}C.

FT-Raman spectra of aqueous solutions of $Mg(NO_3)_2$ and $Mg(OAc)_2$ were recorded at room temperature (28 °C) using a Bruker IFS 66 V optical bench with a FRA 106 Raman module attachment and an Nd:YAG laser operating at 1064 nm. Laser power was set at 200 mW and 250 scans were accumulated and averaged with a resolution of 2 cm^{-1}. The spectra were recorded at the Sophisticated Analytical Instrumentation Facility, Indian Institute of Technology, Madras, India.

3. Computational Details

Classical molecular dynamics simulations of concentrated solutions of magnesium nitrate and magnesium acetate were performed. The unit cell contained 863 water molecules, 4 or 16 magnesium cations and 8 or 32 nitrate or acetate anions, which corresponds to 0.25 or 1 M salt concentration. The size of the cubic unit cell was approximately 30 x 30 x 30 Å and standard periodic boundary conditions were applied.[43] A 12 Å cutoff was used for intermolecular interactions. Long-range Coulomb interactions were accounted for using the particle mesh Ewald procedure.[44] Simulations were run in the NPT canonical ensemble at 300 K and 1 atm. A time step of 1 fs was employed and all bonds involving hydrogen atoms were constrained using the SHAKE algorithm.[45] All systems were first equilibrated for 500 ps, after which a 1 ns production run followed.

A non-polarizable force field was employed in all simulations. Technically, this is the simplest way to avoid the problem of polarization catastrophe,[46] which is

particularly severe in the presence of multiply charged ions. Physically, this choice can be at least partially justified by the fact, that in this study we are interested in bulk properties of aqueous ions, which are less influenced by specific polarization effects than the interfacial ionic behavior.[47] For water, we employed the SPCE model, which accounts for mean polarization effects by increasing the partial charges on oxygen and hydrogens.[48] For ions we used the general amber force field parameter set.[49] For Mg^{2+}, which is missing from this set, we employed OPLS parameters.[50] Partial charges for acetate and nitrate were evaluated using the standard RESP procedure employing the Gaussian 03 program[51] and all MD simulations were performed using the Amber 8 program.[52] To directly check the effect of polarization interaction, we have, however, performed also several test calculations employing a polarizable force field[53,54] with an imposed cutoff on induced dipoles in order to avoid the polarization catastrophe[55] and compared them to non-polarizable simulations.

4. Results and Discussion

4.1. Densities and Isentropic Compressibilities

Within the limited temperature range investigated, the measured densities, ρ, of aqueous solutions of $Mg(NO_3)_2$ and $Mg(OAc)_2$ are found to vary linearly with temperature at a fixed concentration. The least−squares fitted values of the parameters of the density equation ($\rho = a - bt$) are listed in Table 2. The present densities at 25 °C agree within ±0.2% with literature[56–58] data for both $Mg(OAc)_2$ and $Mg(NO_3)_2$ solutions. The corresponding ultrasonic velocities, u, are collected in Table 1S (*Supplementary Information*) and are comparable within ±0.2% for $Mg(OAc)_2$(aq) and ±0.4% for $Mg(NO_3)_2$(aq) with literature[56,59] data at 25 °C.

Table 2. Least−Squares Fitted Values of the Density Equation, $\rho = a - bt$ for Aqueous Solutions of $Mg(OAc)_2$ and $Mg(NO_3)_2$ up to near−saturation concentrations

m/(mol kg^{-1})	a/(kg m^{-3})	b/(kg m^{-3} K^{-1})	std dev in ρ/(kg m^{-3})
	Magnesium Acetate		
0.0414	1010.1 ± 0.4	0.3772 ± 0.0107	0.2
0.0831	1012.9 ± 0.5	0.3686 ± 0.0120	0.2
0.1671	1018.6 ± 0.5	0.3541 ± 0.0132	0.3

0.4247	1038.0 ± 0.4	0.3667 ± 0.0115	0.3
0.6460	1054.4 ± 0.4	0.3898 ± 0.0093	0.2
0.8751	1068.4 ± 0.4	0.3800 ± 0.0113	0.3
1.106	1085.3 ± 0.4	0.4046 ± 0.0102	0.2
1.354	1099.3 ± 0.4	0.4075 ± 0.0101	0.2
1.608	1116.0 ± 0.3	0.4408 ± 0.0086	0.2
1.866	1128.9 ± 0.3	0.4331 ± 0.0085	0.2
2.134	1144.2 ± 0.3	0.4603 ± 0.0078	0.2
2.411	1159.4 ± 0.4	0.4647 ± 0.0100	0.2
2.622	1168.9 ± 0.3	0.4932 ± 0.0083	0.2
3.043	1188.1 ± 0.3	0.5109 ± 0.0068	0.1
3.437	1209.8 ± 0.2	0.5456 ± 0.0066	0.1
3.819	1222.8 ± 0.3	0.5775 ± 0.0078	0.2
4.547	1248.5 ± 0.2	0.6190 ± 0.0056	0.1
5.165	1269.1 ± 0.3	0.6599 ± 0.0066	0.1
5.732	1285.6 ± 0.2	0.6810 ± 0.0064	0.1
6.187	1300.4 ± 0.2	0.7305 ± 0.0034	0.1
6.545	1309.1 ± 0.2	0.7519 ± 0.0048	0.1

Magnesium Nitrate

0.0145	1008.0 ± 0.5	0.3686 ± 0.0130	0.2
0.0528	1012.2 ± 0.4	0.3682 ± 0.0109	0.2
0.2491	1034.3 ± 0.4	0.4106 ± 0.0114	0.2
0.3405	1042.0 ± 0.4	0.3869 ± 0.0101	0.2
0.5931	1068.2 ± 0.3	0.4287 ± 0.0087	0.2
0.6173	1072.0 ± 0.3	0.4542 ± 0.0062	0.1
0.8960	1099.2 ± 0.3	0.4696 ± 0.0074	0.1
0.9898	1109.0 ± 0.3	0.4884 ± 0.0067	0.1
1.262	1133.7 ± 0.3	0.5079 ± 0.0077	0.1
1.525	1157.2 ± 0.1	0.5270 ± 0.0031	0.1
1.694	1172.8 ± 0.2	0.5444 ± 0.0045	0.1
1.827	1186.2 ± 0.2	0.5611 ± 0.0052	0.1
2.131	1211.3 ± 0.2	0.5659 ± 0.0047	0.1
2.493	1240.1 ± 0.2	0.5918 ± 0.0060	0.1
2.584	1248.5 ± 0.1	0.5943 ± 0.0040	0.1
2.793	1264.2 ± 0.1	0.6039 ± 0.0034	0.1
3.096	1287.0 ± 0.1	0.6177 ± 0.0040	0.1
3.118	1288.1 ± 0.2	0.6219 ± 0.0048	0.1
3.170	1296.7 ± 0.2	0.6169 ± 0.0043	0.1
3.501	1315.2 ± 0.1	0.6242 ± 0.0043	0.1
3.704	1329.0 ± 0.1	0.6338 ± 0.0032	0.1
3.757	1332.3 ± 0.1	0.6388 ± 0.0028	0.1
4.039	1350.0 ± 0.1	0.6441 ± 0.0032	0.1
4.051	1349.5 ± 0.1	0.6269 ± 0.0033	0.1
4.285	1366.4 ± 0.1	0.6422 ± 0.0029	0.1
4.403	1373.6 ± 0.1	0.6475 ± 0.0020	0.1
4.728	1395.4 ± 0.1	0.6532 ± 0.0027	0.1
4.883	1402.2 ± 0.1	0.6569 ± 0.0025	0.1
4.970	1408.4 ± 0.1	0.6579 ± 0.0027	0.1
5.134	1419.6 ± 0.2	0.6668 ± 0.0049	0.1

5.282	1427.2 ± 0.5	0.6401 ± 0.0127	0.2

Isentropic compressibilities, $\kappa_{s,}$ of $Mg(OAc)_2$(aq) and $Mg(NO_3)_2$(aq) were calculated using:

$$\kappa_s = (u^2\rho)^{-1} \quad (1)$$

and are plotted against concentration for three temperatures in Figure 1. An empirical equation[40,41] was used to describe the κ_s values:

$$\kappa_s = a_1 + b_1 m + c_1 m^{1.5} + d_1 m^2 + e_1 m^{2.5} + f_1 m^3 \quad (2)$$

where a_1, b_1, c_1, d_1, e_1 and f_1 are temperature–dependent parameters and m is the concentration in mol kg^{-1}. The parameters so obtained are summarised in Table 3.

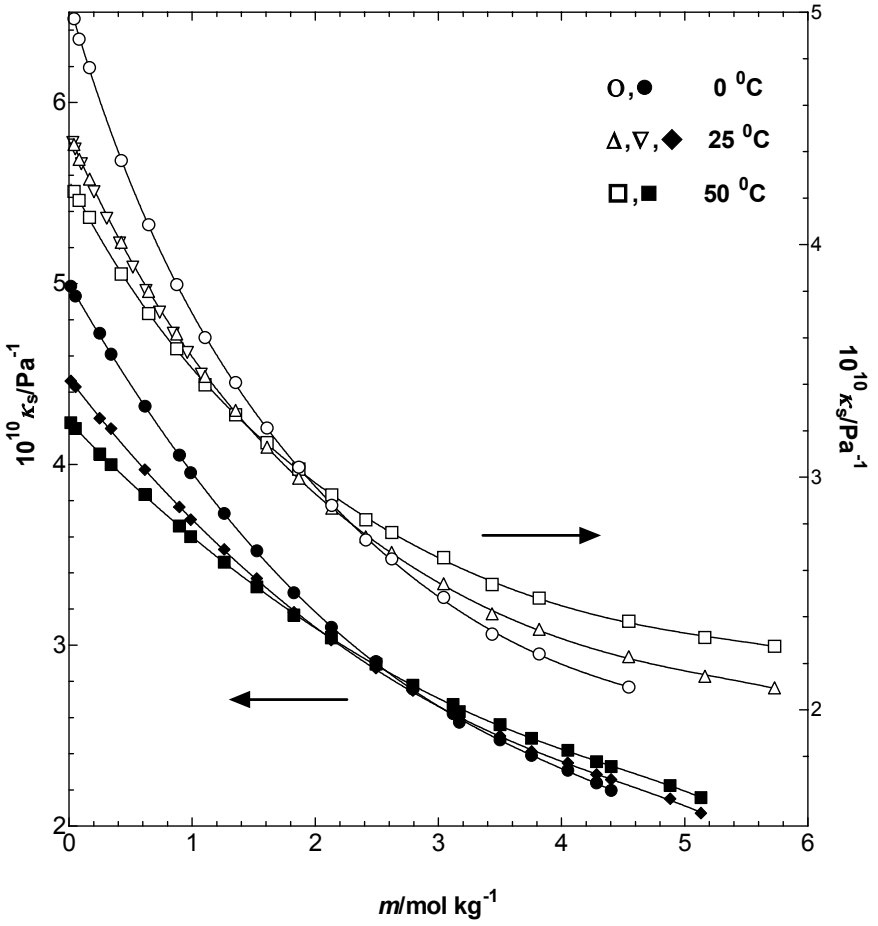

Figure 1. Isentropic compressibilities of aqueous solutions of $Mg(OAc)_2$ (open symbols) and $Mg(NO_3)_2$ (solid symbols) as a function of concentration and temperature. Solid curves are calculated from eq. 2; ∇ ref. 56.

Table 3. Values of the Parameters of eq. 2 for Aqueous Solutions of $Mg(OAc)_2$ and $Mg(NO_3)_2$

Parameters	0 °C	25 °C	50 °C
	Magnesium Acetate		
$10^{10}a_1$ /Pa^{-1}	5.0403 ± 0.0076	4.4759 ± 0.0059	4.2758 ± 0.0057
$10^{10}b_1$ /Pa^{-1} kg mol^{-1}	-1.8405 ± 0.0459	-1.2317 ± 0.0268	-1.0471 ± 0.0259
$10^{10}c_1$ / Pa^{-1} kg$^{1.5}$ mol$^{-1.5}$	0.6508 ± 0.0713	0.3344 ± 0.0326	0.2954 ± 0.0314
$10^{10}d_1$ /Pa^{-1} kg^2 mol^{-2}	-0.1728 ± 0.0424	-0.0690 ± 0.0153	-0.0636 ± 0.0147
$10^{10}e_1$ / Pa^{-1} kg$^{2.5}$ mol$^{-2.5}$	0.0271 ± 0.0106	0.0093 ± 0.0030	0.0086 ± 0.0029
$10^{12}f_1$ /Pa^{-1} kg^3 mol^{-3}	-0.0017 ± 0.0009	-0.0005 ± 0.0002	-0.0005 ± 0.0002
$10^{10}\sigma$	0.0075	0.0066	0.0064
	Magnesium Nitrate		
$10^{10}a_1$ /Pa^{-1}	5.0008 ± 0.0067	4.4750 ± 0.0611	4.2374 ± 0.0050
$10^{10}b_1$ /Pa^{-1} kg mol^{-1}	-1.1907 ± 0.0391	-0.8908 ± 0.0302	-0.7278 ± 0.0248
$10^{10}c_1$ / Pa^{-1} kg$^{1.5}$ mol$^{-1.5}$	0.1115 ± 0.0011	0.1273 ± 0.0407	0.1106 ± 0.0334
$10^{10}d_1$ /Pa^{-1} kg^2 mol^{-2}	-0.0011 ± 0.0367	-0.0199 ± 0.0210	-0.0262 ± 0.0173
$10^{10}e_1$ / Pa^{-1} kg$^{2.5}$ mol$^{-2.5}$	0.0009 ± 0.0094	0.0044 ± 0.0046	0.0062 ± 0.0038
$10^{12}f_1$ /Pa^{-1} kg^3 mol^{-3}	-0.0002 ± 0.0008	-0.0004 ± 0.0004	-0.0006 ± 0.0006
$10^{10}\sigma$	0.0075	0.0071	0.0058

It is apparent from Figure 1 that the κ_s isotherms for each electrolyte within the studied temperature range (0 to 50 °C) exhibit a crossover at an approximately constant concentration that appears to be characteristic. As the electrolyte concentration increases, κ_s decreases due to the simultaneous effects of ion hydration and the breaking of the extended molecular organisation of water. The main contributor to these effects would be expected to be Mg^{2+} because of its higher charge density and hydration energy.[60]

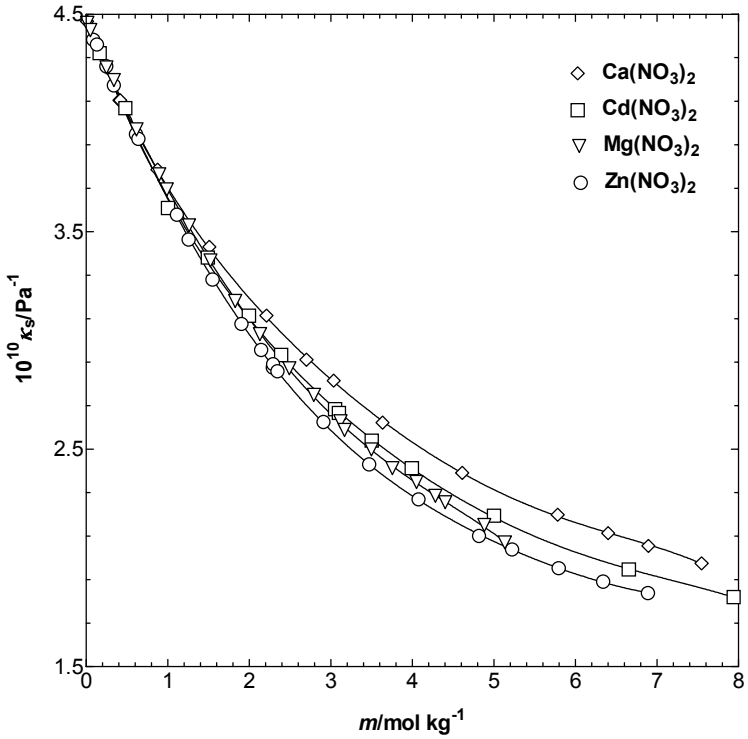

Figure 2. Isentropic compressibilities of various aqueous solutions of NO_3^- salts as a function of concentration at 25 °C: O ref. 40; □, ◊ ref. 41.

The influence of cation size (charge density) on κ_s is illustrated in Figure 2, which plots data for various $M(NO_3)_2$(aq) solutions at 25 °C. As would be expected from the greater electrostriction[61] associated with decreasing cationic radii (r),[62] the κ_s values at higher solute concentrations decrease in the order: Zn^{2+} (r = 0.74 Å) < Cd^{2+} (r = 0.95 Å) < Ca^{2+} (r = 0.99 Å), with Mg^{2+} (r = 0.65 Å) as a partial exception. The anomalous position of Mg^{2+} disappears if the M^{2+}–OH_2 distances (d) are used instead of the radii (d = 2.44, 2.31, 2.12 and 2.04 pm for M = Ca, Cd, Zn and Mg, respectively).[63]

On the other hand, comparison of the effects of OAc^- and NO_3^- on κ_s values is less straightforward. Figure 3 shows that $Mg(OAc)_2$ solutions are less compressible than $Mg(NO_3)_2$ solutions up to ≈ 4.6 mol kg^{-1} at 25 °C but this is reversed at higher concentrations. For comparison, κ_s data for $MgCl_2$ and $MgSO_4$ solutions[64] are also included in Figure 3. Taking these data at face value, i.e., ignoring the crossover and ionic strength differences, there is again a reasonable correlation between charge density (which, invoking the Drude–Nernst equation,[61] can be taken as z^2/r) and the κ_s

values, which are in the order SO_4^{2-} (z^2/r =1.74 Å^{-1}) << Cl^- (z^2/r = 0.55 Å^{-1}) ≈ NO_3^- (z^2/r = 0.56 Å^{-1}) with OAc^- (z^2/r = 0.43 Å^{-1}) as a partial exception, assuming $r(SO_4^{2-})$ = 2.30 Å, $r(OAc^-)$ = 2.32 Å, $r(Cl^-)$ = 1.81 Å and $r(NO_3^-)$ = 1.79 Å.[65] In contrast with the cations, the κ_S values do not correlate with the anion-water distances [$d(SO_4^{2-}$–$(H_2)O)$ = 3.70 Å, $d(OAc^-$–$(H_2)O)$ = 3.70 Å, $d(Cl^-$–$(H_2)O)$ = 3.15 Å, $d(NO_3^-$–$(H_2)O)$ = 3.40 Å] obtained from diffraction studies.[12,13] However, this might be expected since the crucial X^{n-}–H distances can only be inferred from XRD studies and neither OAc^- nor NO_3^- are symmetrical.

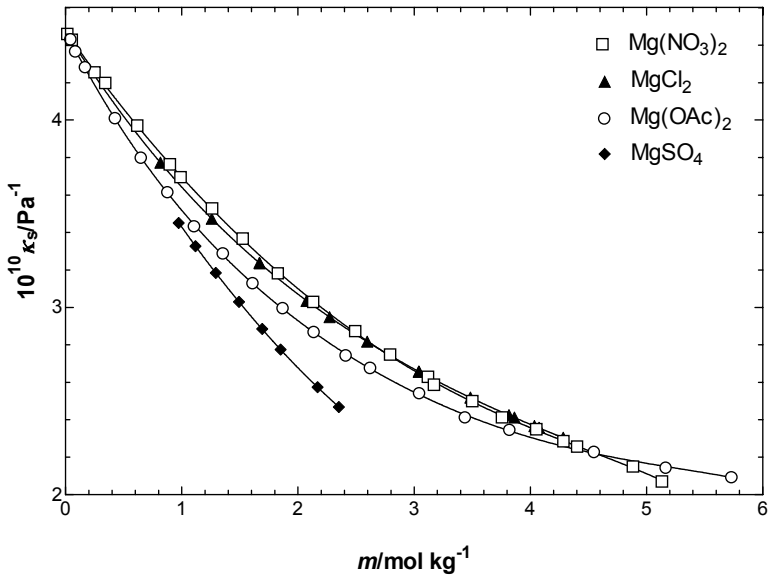

Figure 3. Isentropic compressibilities of aqueous solutions of various Mg^{2+} salts as a function of concentration at 25 ^{0}C: ▲, ♦ ref. 64.

On the other hand, it is noteworthy that the κ_S data as presented appear to conform to the Hofmeister series.[36] Thus, OAc^- and SO_4^{2-} belong to the salting-out side, Cl^- is in the middle and NO_3^- belongs to the salting-in side of the series. On this basis, $Mg(OAc)_2$ and $Mg(NO_3)_2$ would be expected to have qualitatively different effects on the water structure. As discussed above (Figure 1), the crossover concentration for $Mg(OAc)_2$(aq) is lower than that for $Mg(NO_3)_2$(aq), which implies that OAc^- is more efficient in disrupting the molecular organisation of water than NO_3^-.

To further investigate possible Hofmeister effects, Figure 4 plots κ_S values at 25 °C for various Na salts.[42,64,66,67] Again taking the data at face value, the trend is consistent with the Hofmeister series.[36]

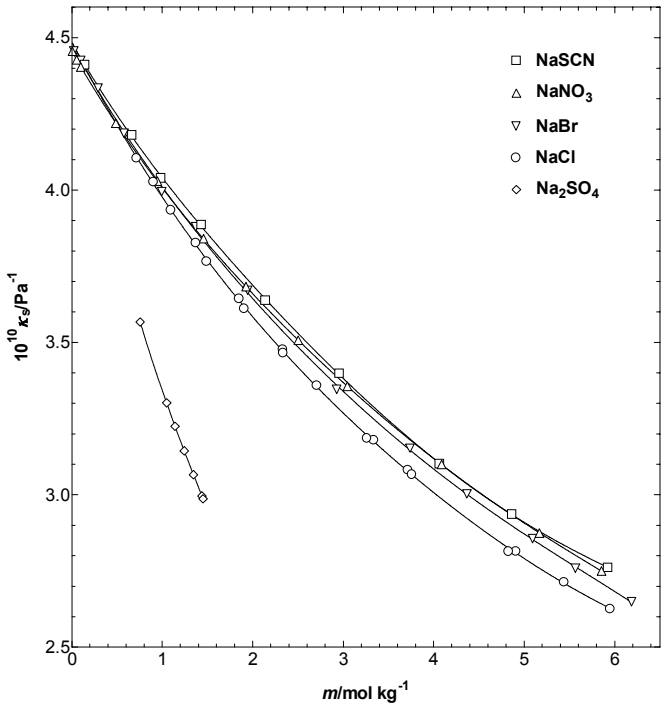

Figure 4. Isentropic compressibilities of aqueous solutions of various Na^+ salts as a function of concentration at 25 °C: □ ref. 42; O, ◊ ref. 64; Δ ref. 66; ∇ ref. 67.

The crossover concentration for κ_S isotherms (Figure 1) can be considered[40,41] as coinciding with the disappearance of the bulk water structure, with all the water molecules being incorporated into the hydration shells of the ions, resulting in a more rigid structure for the solution. Beyond this concentration, the co-spheres of the cations and anions overlap leading to the formation of ion pairs.[68] Figure 1 shows that the κ_S isotherms for $Mg(OAc)_2$ and $Mg(NO_3)_2$ solutions do not cross at a fixed concentration but rather over narrow concentration ranges (1.50–2.30 mol kg^{-1} and 2.00–3.00 mol kg^{-1}, respectively) within the temperature range of study. So, to identify the concentration at which the total hydration number of a solute would be realised and at a fixed temperature, the temperature derivative plot of κ_S isotherm for both the systems appears to be an essential step. We prefer to estimate the total hydration number at 25 °C and for the purpose the temperature derivative plot of κ_S isotherm for both systems is shown in Figure 5. A two-degree polynomial equation was used to fit the data.

Evidently, the $d\kappa_s/dt$ plots become zero at 2.28 mol kg^{-1} and 2.90 mol kg^{-1}, respectively, for $Mg(OAc)_2$ and $Mg(NO_3)_2$ solutions.

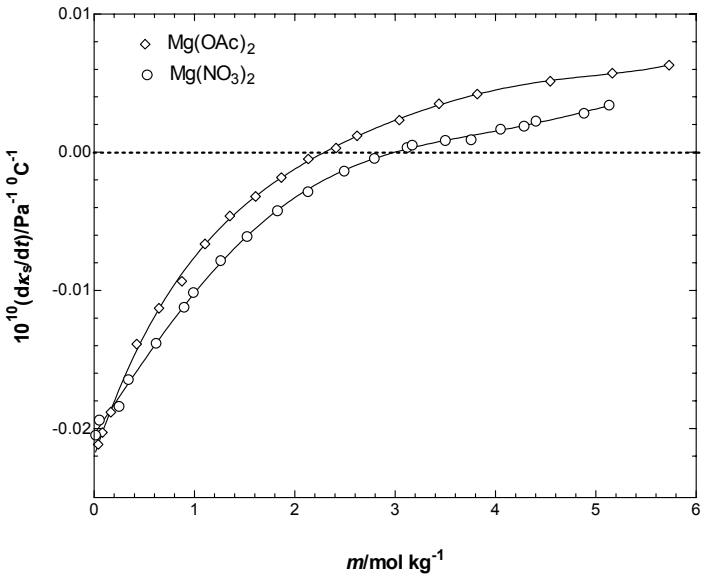

Figure 5. Temperature derivative of the isentropic compressibility as a function of concentration for aqueous solutions of $Mg(OAc)_2$ and $Mg(NO_3)_2$ at 25 °C.

The total hydration numbers, n_h, of $Mg(OAc)_2$(aq) and $Mg(NO_3)_2$(aq) can be calculated using the empirical equation:[40–42]

$$n_h = (\kappa_{s,\phi} - \kappa_{s,h}V_\phi)/[V_1(\kappa_{s,h} - \kappa_{s,1})] \quad (3)$$

where $\kappa_{s,\phi}$ is the apparent molal isentropic compressibility of the solute, $\kappa_{s,h}$ is the isentropic compressibility of the hydration shell of the solute, V_ϕ is the apparent molal volume of the solute and $\kappa_{s,1}$ and V_1 are the isentropic compressibility and the molar volume of the solvent, respectively. Using this expression, the total hydration numbers for $Mg(OAc)_2$ and $Mg(NO_3)_2$ solutions were estimated to be 24.3 and 19.2 at 2.28 mol kg^{-1} and 2.90 mol kg^{-1}, respectively.

4.2. Structural Relaxation Times

The measured viscosities for aqueous solutions of $Mg(NO_3)_2$ and $Mg(OAc)_2$ are collected in Table 2S (*Supplementary Information*). The present data for $Mg(NO_3)_2$(aq)

are within ±5% of the literature values.[57,58] No previous viscosity data appear to have been published for $Mg(OAc)_2$(aq).

To help understand the nature of ionic interactions at different concentrations, the structural relaxation time, τ, was calculated using:

$$\tau = 4\kappa_S \eta/3 \qquad (4)$$

The quantity τ can be considered as the time required to release the shear stress at constant strain through viscous flow. It is particularly sensitive to the formation of ion pairs because of coupling between ion–solvent and ion–ion interactions. Figure 6 shows the variation of τ with concentration at three temperatures for aqueous solutions of $Mg(NO_3)_2$ and $Mg(OAc)_2$.

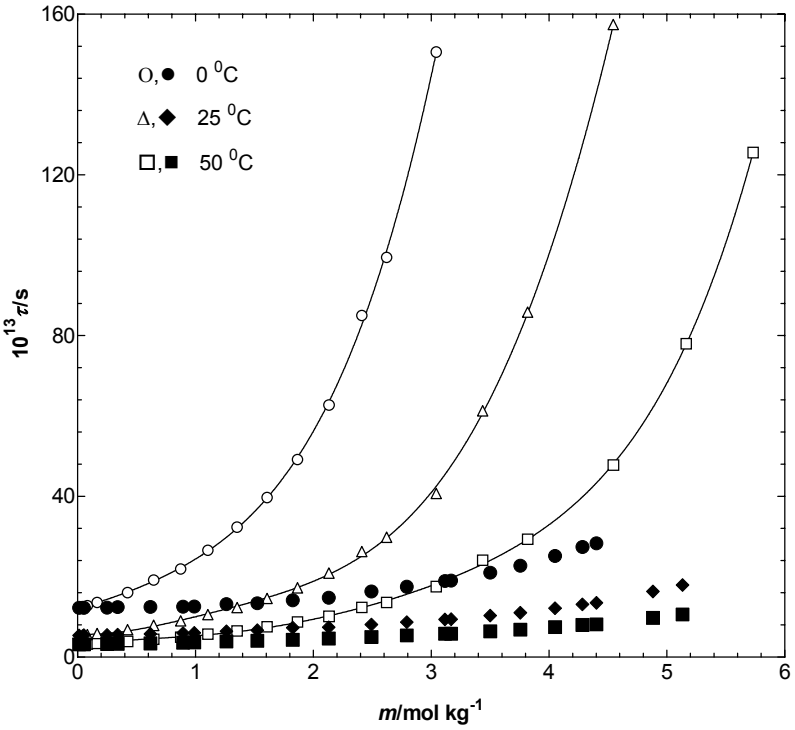

Figure 6. Variation of the structural relaxation time, τ, with concentration for aqueous solutions of $Mg(OAc)_2$ (open symbols) and $Mg(NO_3)_2$ (solid symbols).

The dramatic differences between the solutions of the two salts almost certainly reflect differences in the extent and nature of their ion association. Although the existing information (Table 1) is somewhat contradictory, there is little doubt that $Mg(OAc)_2(aq)$ is not only more strongly associated than $Mg(NO_3)_2(aq)$ but also that it forms more contact (inner sphere) species. These issues will be discussed further below when considering the Raman spectra.

4.3. Electrical Conductivities

If ion pair formation in $Mg(OAc)_2(aq)$ is significantly greater than in $Mg(NO_3)_2(aq)$, significant effects would be expected on ionic mobilities, i.e., on their electrical conductivities. Experimental specific electrical conductivities, κ, for aqueous solutions of $Mg(OAc)_2$ and $Mg(NO_3)_2$ are listed in Table 3S (*Supplementary Information*). The data are around 3–6%[69a] and 1–10%[69b], respectively, lower than the literature values at 25 °C.

Figure 7 plots κ vs. m for solutions of the two salts at three temperatures. All the κ isotherms pass through a maximum (κ_{max}), which is located at 1.07 ± 0.13 mol kg^{-1} and 2.45 ± 0.09 mol kg^{-1} for the acetate and nitrate salts, respectively. At higher concentrations (> 1 mol kg^{-1}) the κ ($Mg(OAc)_2(aq)$) is substantially smaller than κ ($Mg(NO_3)_2(aq)$). Although a small part of these differences can be attributed to the greater mobility of NO_3^-, $\lambda^o(NO_3^-)$ = 71.5 cm^2 S mol^{-1}, than that of OAc^-, $\lambda^o(OAc^-)$ = 40.9 cm^2 S mol^{-1};[70] the greatest part is almost certainly due the higher level of ion pair formation in $Mg(OAc)_2(aq)$.

The reasons why OAc^- should associate with Mg^{2+} more strongly than NO_3^- are undoubtedly complicated. In addition to long range electrostatic interactions, short range covalent and polarization effects are probably important. The effects of solvation must also be considered. Because of their very different structures and chemical characteristics, the interactions of OAc^- and NO_3^- with water molecules differ considerably. In the Hofmeister series, OAc^- lies toward the salting–out end whereas NO_3^- is towards the salting–in end, which indicates a very different interaction of the

two ions with solvent water. Acetate is hydrated by six water molecules[29] and is thought to modify the structure of water in a similar manner to alcohols,[71] probably due to the presence of its hydrophobic part. On the other hand, NO_3^- forms a H-bonded complex with two water molecules having two dominant structures.[72] It may be that the hydrophobic end of the CH_3COO^- ion promotes its entry into the primary hydration shell of Mg^{2+}, however, it should be noted that the 'absolute' Gibbs energy of hydration for OAc^- is ≈ 60 kJ mol^{-1} more negative (i.e., more favourable) than that of NO_3^-.[65]

The differences between $Mg(OAc)_2(aq)$ and $Mg(NO_3)_2(aq)$ for both τ (Figure 6) and κ (Figure 7) become more pronounced at lower temperatures, which suggests that ion pairing in the former increases with decreasing temperature. This is consistent with the measured negative enthalpy of complexation.[73] It is interesting to note that the concentration corresponding to κ_{max} for $Mg(NO_3)_2$ solutions coincides with the κ_s crossover. This is consistent with the presence of at least some type (probably non-contact) of ion pairs at higher concentrations.

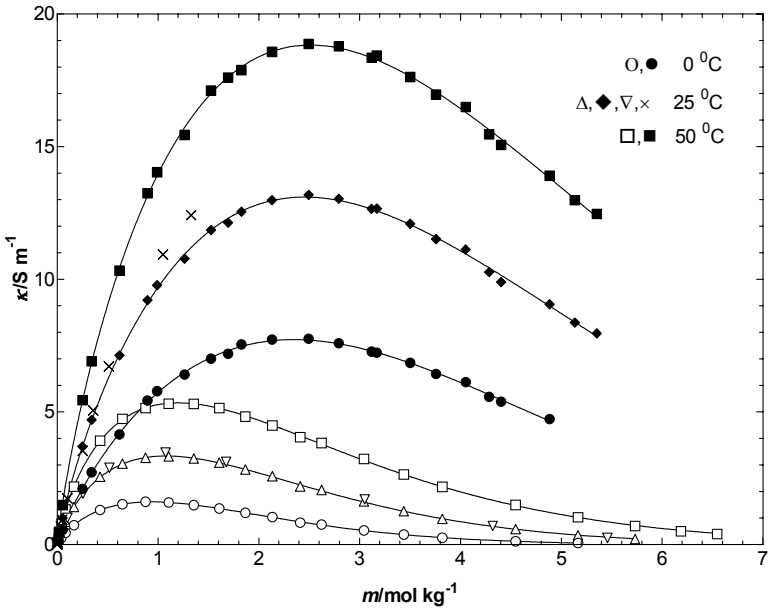

Figure 7. Variation of electrical conductivity with concentration for aqueous solutions of $Mg(OAc)_2$ (open symbols) and $Mg(NO_3)_2$ (solid symbols) at three temperatures;∇ ref. 69*a*; × ref. 69*b*.

4.4. FT-Raman Spectra

4.4.1 Magnesium Acetate Solutions

The Raman spectra for $Mg(OAc)_2(aq)$ are presented at various concentrations in Figure 8. The band positions associated with OAc^- are summarised in Table 4. Band assignments are based on those of previous investigations.[8,32–35] The antisymmetric stretching mode (ν_8) is only very weakly observed in Raman spectra and so will not be considered further.

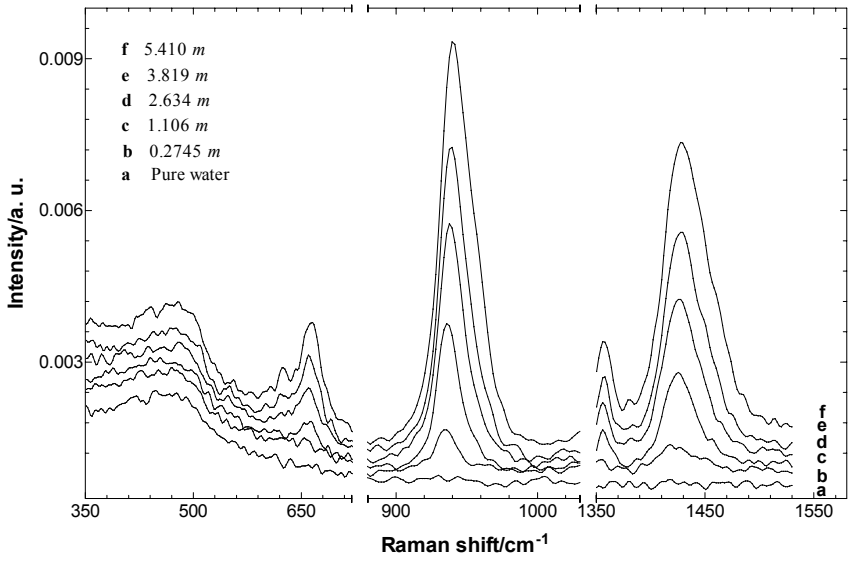

Figure 8. Raman spectra of aqueous solutions of $Mg(OAc)_2$ and pure water at room temperature.

Table 4. Peak positions and assignment of modes associated with the acetate ion in aqueous solutions of $Mg(OAc)_2$

m/mol kg^{-1}	Peak position/cm^{-1}				
	COO^- in-plane rock (ν_{11})	COO^- deformation (ν_5)		C–C stretch[a] (ν_4)	COO^- symmetric stretch[a] (ν_3)
0.2745		654		935 (17)	1418 (32)
1.106		658		936 (19)	1425 (34)
2.634	480	660	621	938 (21)	1426 (39)
3.819	479	661	621	939 (24)	1428 (42)
5.410	479	666	624	940 (28)	1428 (45)

[a]The values in parentheses represent the full width at half maximum height (fwhh) for the given band

The broad COO^- symmetric stretching mode (ν_3) of OAc^-, which appears in the 1400–1500 cm^{-1} region (Figure 8), lies very close to, and contains contributions from, the CH_3 deformation modes ν_9 and ν_{13}.[33,35,74] This band shows a blue shift, with increasing intensity on the high frequency side at higher salt concentrations, which is reflected in an increase in the full-width at half (maximum) height (fwhh) of the band (Table 4). At 5.410 mol kg^{-1}, two wings on the high frequency side of this band are apparent at ~1445 and ~1463 cm^{-1}. The ν_3, ν_9 and ν_{13} modes for solid $Mg(OAc)_2{\cdot}4H_2O$ also overlap. The resolved component bands were found to appear at 1436–1438 cm^{-1}, 1420–1421 cm^{-1} and 1446–1455 cm^{-1}, respectively.[33,74] In the solid phase, a bisacetato complex is the building unit for $Mg(OAc)_2$.[74,75]

As the CH_3 deformation modes (ν_9 and ν_{13}) are not sensitive to the metal-carboxyl group interactions, the observed frequency shift ($\Delta\nu_3 \sim 10$ cm^{-1}) and the increasing asymmetry of the band on the high frequency side can be attributed to changes in the COO^- stretching vibration due to complexation with Mg^{2+}. Further, the appearance of the two high frequency wings at 5.410 mol kg^{-1}, suggests the occurrence of both mono- and bidentate complexes. Wang et al.[35] also observed two shoulders in ν_3 Raman mode at ~1456 and 1443 cm^{-1} at $m \geq 3.58$ mol kg^{-1} for $Mg(OAc)_2$(aq) and attributed them to bidentate and bridged bidentate complexes, respectively. Nickolov et al.[33] employed band fitting techniques to the Raman spectra of $Mg(OAc)_2$(aq) and reported that bisacetato complexes were the dominant species in saturated solutions.

The C–C stretching band (ν_4) of OAc^- is probably the most useful with respect to establishing the existence of metal-acetato complexes.[33–35,74] It has a high Raman scattering coefficient and does not overlap with other vibrations. In the present spectra (Figure 8) it occurs as a reasonably sharp band, centred at ~938 cm^{-1}. As the solute concentration increases, this band shows a small blue shift (Table 4) and a simultaneous development of asymmetry on the high frequency side with a weak shoulder at ~948 cm^{-1}. The ν_4 band is observed at 892 cm^{-1} for HOAc and at 928 cm^{-1} for free OAc^-(aq).[34] For $Mg(OAc)_2{\cdot}4H_2O$(s) the band occurs at 947 cm^{-1}.[33] The variation in the position of the ν_4 mode with concentration suggests the formation of mono- and bidentate contact ion pairs (inner–sphere complexes) at higher concentrations. Similar

observations for $Mg(OAc)_2(aq)$ have been made by Nickolov et al.[33] They resolved the ν_4 band into three components at 930 cm^{-1}, 939 cm^{-1} and 947 cm^{-1} by curve fitting methods and ascribed them to free OAc^-, monoacetato complexes and bisacetato complexes, respectively. A blue shift of the ν_4 band from 936 to 947 cm^{-1} with increasing concentration of $Mg(OAc)_2(aq)$ was ascribed to the transformation of free OAc^- to contact ion pairs between Mg^{2+} and OAc^-.[35] Semmler et al.[8] suggested the formation of monoacetato complexes in $Mg(OAc)_2(aq)$ and were able to resolve a band at 939 cm^{-1} above 100 °C.

Additional evidence in support of complex formation in $Mg(OAc)_2$ solutions can be derived from the COO^- deformation or bending (ν_5) and in-plane rocking (ν_{11}) modes.[74] In the present spectra (Figure 8), ν_5 was observed at 654 cm^{-1} for a 0.2745 mol kg^{-1} solution, shifting to 666 cm^{-1} at 5.410 mol kg^{-1}. Such a large blue shift can be attributed to the complexation of COO^- with Mg^{2+}. However, at $m \geq 2.634$ mol kg^{-1} a shoulder appears at ~621 cm^{-1}, ultimately producing a peak at 624 cm^{-1} at $m = 5.410$ mol kg^{-1}. The appearance of two ν_5 bands is consistent with their observation (at 678 and 612 cm^{-1}) for solid $Mg(OAc)_2$ at liquid nitrogen temperature.[74] This suggests that the 624 cm^{-1} band may originate from bidentate complexes.[35]

A broad envelope at 400–500 cm^{-1}, corresponding to the ν_{11} mode, is observed (Figure 8) in the present spectra of $Mg(OAc)_2(aq)$. This band probably overlaps with the water libration band, which occurs at ~450 cm^{-1}.[76] At higher concentrations (≥ 2.634 mol kg^{-1}) the ν_{11} band becomes prominent at ~479 cm^{-1}. Its broadness suggests the presence of various environments for the COO^- moiety. At 5.410 mol kg^{-1}, an additional shoulder at ~496 cm^{-1} is apparent. This is identical to that reported for solid $Mg(OAc)_2 \cdot 4H_2O$,[33] which implies the presence of bisacetato complexes. A shift of the ν_{11} mode from 480 to 510 cm^{-1} for aqueous $Ni(OAc)_2$ solutions has been ascribed to complex formation.[77]

4.4.2. Magnesium Nitrate Solutions

Raman spectra of $Mg(NO_3)_2$(aq) are depicted in Figure 9. Unperturbed NO_3^- has D_{3h} symmetry and gives rise to symmetric stretching (ν_1), out-of-plane deformation (ν_2), asymmetric stretching (ν_3) and in-plane deformation or bending (ν_4) modes.[21,22] The ν_3 and ν_4 modes are both Raman and IR active whereas the ν_1 is Raman active only and ν_2 is IR active only. The band positions for NO_3^- in the present $Mg(NO_3)_2$ solutions are summarised in Table 5.

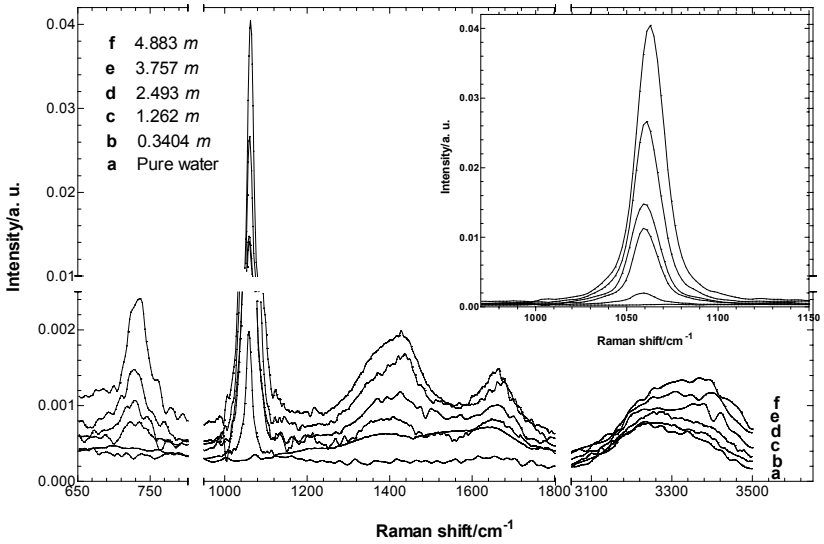

Figure 9. Raman spectra of aqueous solutions of $Mg(NO_3)_2$ and pure water at room temperature.

Table 5. Assignment of modes and peak positions associated with the nitrate ion in aqueous solutions of $Mg(NO_3)_2$

m/ mol kg^{-1}	Peak position/cm^{-1}				
	in-plane deformation (ν_4)	symmetric[a] stretch (ν_1)	asymmetric stretch (ν_3)	water O–H stretch	
0.3404	726	1059 (16)	1390	3234	3385
1.262	728	1059 (17)	1408	3259	3390
2.493	729	1059 (19)	1421	3254	3368
3.757	728	1061 (18)	1427	3260	3398
4.883	734	1063 (20)	1428	3264	3390

[a]The values in the parentheses represent fwhh

The inset in Figure 9 shows the variation of the ν_1 mode with increasing salt concentration. The intensity and the fwhh of this band increase as the concentration increases. The band position is constant at 1059 cm^{-1} up to 2.493 mol kg^{-1} but blue shifts by 4 cm^{-1} at higher concentrations. There is also a slight increase in fwhh (Table

5), which has been attributed[27] to the influence of hydrated cations on NO_3^-. This implies the presence of non-contact ion pairs at high $Mg(NO_3)_2$ concentrations. Previous principal component analysis[25] of the Raman spectra of $Mg(NO_3)_2$(aq) indicated the presence of some associated species probably solvent-shared ion pair at ≥ 2.5 mol dm^{-3}.

Zhang et al.,[23] in their study of highly concentrated droplets of $Mg(NO_3)_2$(aq) using Raman microscopy, observed that ν_1 shifted from 1049 cm^{-1} to 1055 cm^{-1} when the concentration changed from 7.60 mol kg^{-1} to 10.09 mol kg^{-1} and suggested it was due to the formation of contact ion pairs. Peleg[21] too reported ν_1 shifted from 1049 cm^{-1} to 1053 cm^{-1} when the $Mg(NO_3)_2$ concentration increased from 9.25 mol kg^{-1} to 13.22 mol kg^{-1} and also invoked contact ion pairs as the explanation. Above 9.25 mol kg^{-1} (in hydrated melts), splitting of the ν_1 band has been reported and was thought to be evidence for the formation of different types of contact ion pairs.[21–23]

Unperturbed NO_3^- gives a single ν_3 band at 1370 cm^{-1}.[71] Previously,[40,41,72,78] it was concluded that water causes splitting of the ν_3 band due to hydration or solvent-shared ion pair formation. For example, bifurcated ν_3 bands appear at ~1341 and ~1402 cm^{-1} in 3.43 mol kg^{-1} $Zn(NO_3)_2$(aq).[40] In the present study, no splitting of ν_3 was observed at lower concentrations and the band profiles matched well with those of Chang and Irish[22] and Zhang et al.[23] Beyond 2.493 mol kg^{-1}, the band intensity increased asymmetrically on the high frequency side and the band maximum occurred at ~1428 cm^{-1} with a shoulder at ~1370 cm^{-1}. Peleg[21] also reported a splitting of the ν_3 band in 2.78 mol kg^{-1} $Mg(NO_3)_2$ solutions. It seems reasonable to ascribe the ~1370 cm^{-1} shoulder to unperturbed NO_3^-[72] and the mode at ~1428 cm^{-1} to NO_3^- perturbed by (or associated with) hydrated cations.[21]

The intensity of the broad band in the 1600–1700 cm^{-1} region increases with concentration. However, as the $2\nu_2$ overtone for NO_3^- at ~1658 cm^{-1} and the water deformation mode (at 1636 cm^{-1}) also occur in this region, no detailed analysis is possible.[21,22]

The appearance of double in-plane deformation bands (ν_4), at ~750 and ~720 cm^{-1}, is considered diagnostic for contact ion pair formation.[20–22] Our $Mg(NO_3)_2$ solutions produced a single Raman band at ~726 cm^{-1} for 0.3404 mol kg^{-1}, which blue shifted by only ~2 cm^{-1} up to 3.757 mol kg^{-1}. The intensity of the band was proportional to the concentration.[22] At 4.883 mol kg^{-1}, the band shows a blue shift of ~8 cm^{-1}, suggesting perturbation of NO_3^- by hydrated Mg^{2+}, as proposed by Angell.[27] The possible mode at ~760 cm^{-1} (Figure 9) may be due to noise, because the 750 cm^{-1} band for $Mg(NO_3)_2$(aq) appears only above 9.25 mol kg^{-1}.[21,22]

The $\nu_{O–H}$ envelope of pure water is thought to consist of four components, an ice-like component (C_1) at ~3230 cm^{-1}, an ice-like liquid component (C_2) at ~3420 cm^{-1}, a liquid-like amorphous phase (C_3) at ~3540 cm^{-1} and monomeric H_2O (C_4) at ~3620 cm^{-1}.[79] In the present systems, $\nu_{O–H}$ mode exhibits one broad peak at ~3234 cm^{-1} with a shoulder at ~3385 cm^{-1}. Upon addition of $Mg(NO_3)_2$, the shoulder grows relative to the ~3234 cm^{-1} band. At 4.883 mol kg^{-1}, the shoulder becomes the main peak. The positive shift of the $\nu_{O–H}$ band maximum has been ascribed to the disruption of the water structure and formation of bonds between water and ions.[80]

In summary, the Raman bands observed at ~726, ~1059 and ~1390 cm^{-1} along with $\nu_{O–H}$ suggest that NO_3^- does not bond directly to Mg^{2+} within the experimental concentration range. Nevertheless, there are changes in the spectra that suggest that non-contact ion pairs may be formed, particularly at high concentrations.

4.5. Mean Distance Between Cation and Anion

To better ascertain the existence of different ionic species in different concentration regions, an attempt was made to determine the maximum possible mean cation–anion distance.[81] Assuming a random distribution of the ions in the solution without any attractive or repulsive interactions, the estimated mean cation–anion distance is depicted in Figure 10 as a function of concentration for both salt systems.

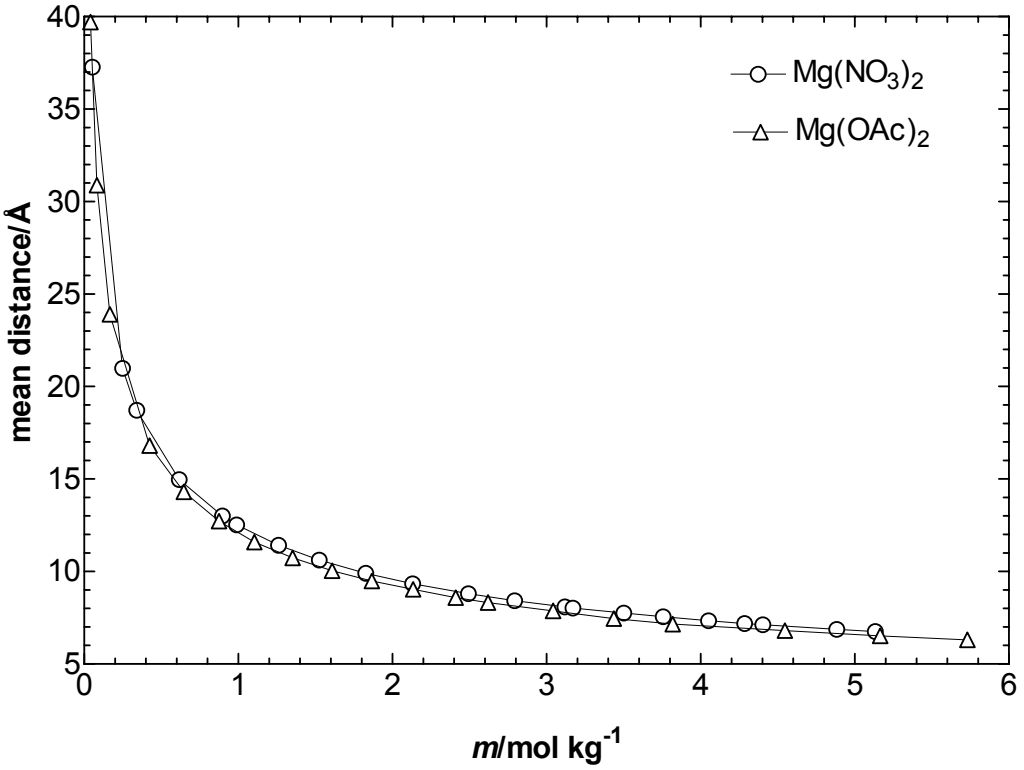

Figure 10. Variation of mean cation–anion distance for $Mg(OAc)_2(aq)$ and $Mg(NO_3)_2(aq)$ with concentration, assuming a random distribution of the ions.

According to this model the mean cation–anion distance decreases sharply up to ≈1.0 mol kg^{-1} but gradually decreases thereafter. A simple geometrical arrangement (Figure 11) illustrates the cation–anion separation, including water molecules: one nominally associated with the cation and another with the anion. For $Mg(OAc)_2(aq)$ the Mg^{2+}–OH_2 and OAc^-–$(H_2)O$ equilibrium distances obtained from X-ray diffraction[12,63] should be taken into account along with the diameter of the water molecules. In Figure 11 the separation is 8.62 Å, which corresponds to the mean distance between the ions at a concentration of 2.37 mol kg^{-1}, if a random distribution without ion–ion interactions is assumed. Similarly for $Mg(NO_3)_2(aq)$, the separation required by two water molecules in between Mg^{2+} and NO_3^- is 8.32 Å, which corresponds to the mean distance at 2.86 mol kg^{-1} (Figure 10). These concentrations, 2.37 and 2.86 mol kg^{-1} for $Mg(OAc)_2$ and $Mg(NO_3)_2$, respectively, are comparable with those at which $d\kappa_s/dt = 0$ (Figure 5), which lends support to the idea that they correspond to the situation in which the available water molecules are just sufficient to complete the hydration shells of the dissolved ions. Above these concentrations solvent–shared or contact ion pair

formation is inevitable, as the mean separation between the ions can no longer accommodate more than one water molecule. It is again emphasised that this conclusion is derived from purely (and 'primitive') geometric considerations. No account has been taken of short-range attractive forces or even of geometric constraints, such as the presence of the CH_3 group in the acetate ion, which might allow its closer approach to Mg^{2+}.[35]

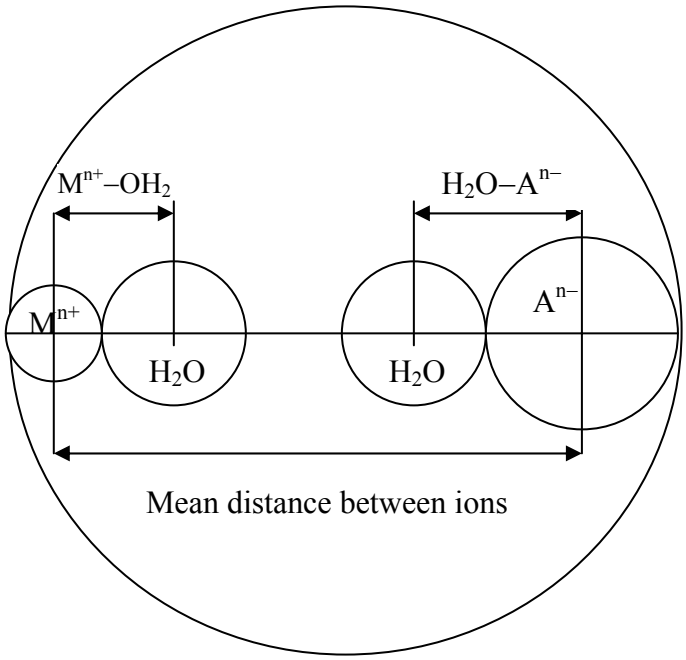

Figure 11. Geometrical representation of the separation between a cation, M^{n+} and an anion, A^{n-} in aqueous solutions.

4.6. Computational Results

Molecular dynamics simulations were used to study hydration and ion pairing in aqueous solutions of magnesium nitrate and acetate, yielding a statistically relevant picture with atomic resolution. Figures 12 and 13 present typical snapshots from simulations of 1 M $Mg(NO_3)_2$(aq) and $Mg(OAc)_2$(aq), which show the qualitative difference between these two salt systems. In $Mg(NO_3)_2$(aq) most of the ions are separated from other ions and are fully hydrated. The opposite is true for $Mg(OAc)_2$(aq), where many of the Mg^{2+} ions are associated with OAc^- ions. Moreover,

a significant degree of ion clustering is observed, particularly around Mg^{2+}, which are associated with more than one OAc^{-}.

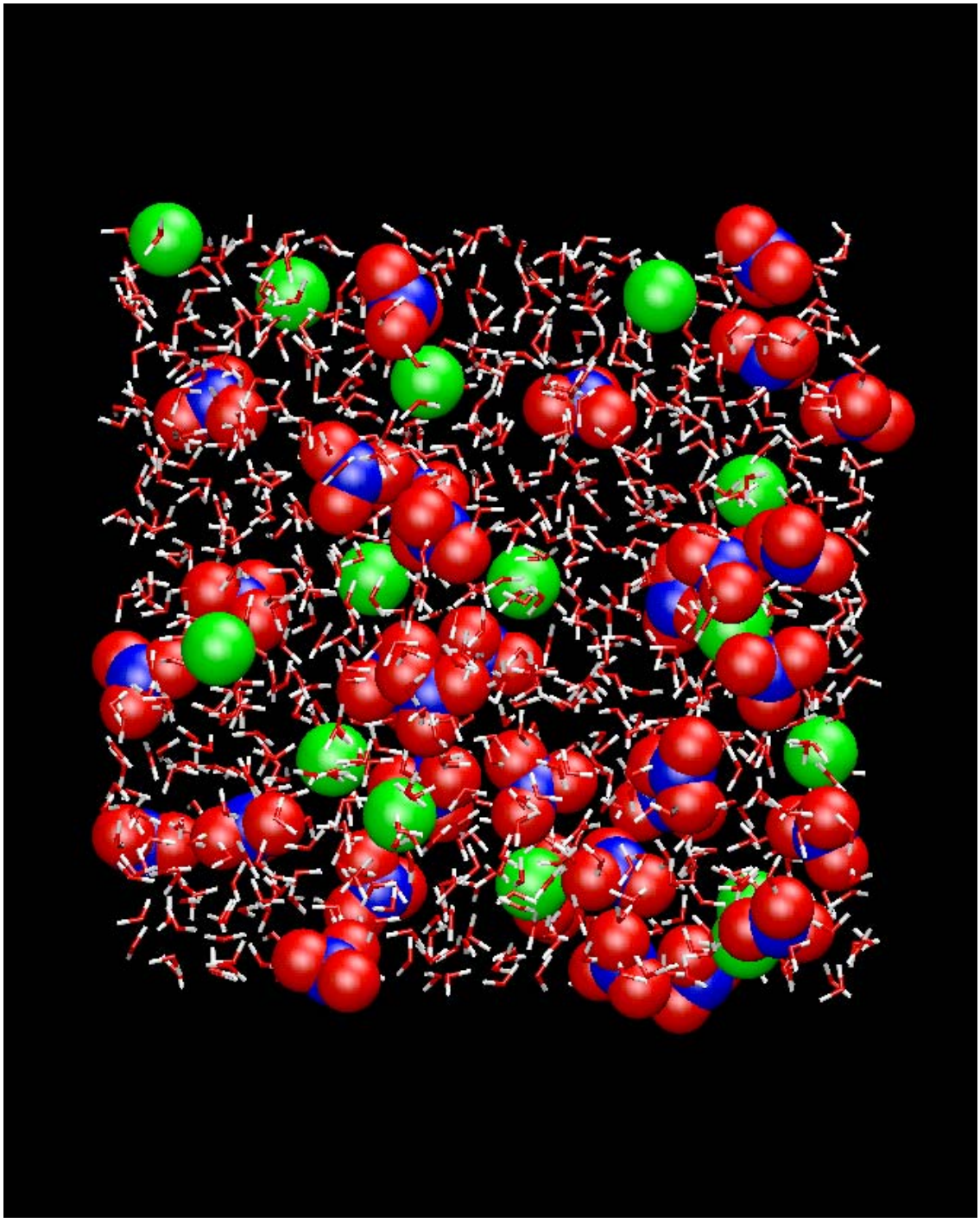

Figure 12. A snapshot from a simulation of 1 M $Mg(NO_3)_2$(aq). Color coding: Mg - green, N - blue, O - red, H - white. For clarity water molecules are displayed in the stick representation.

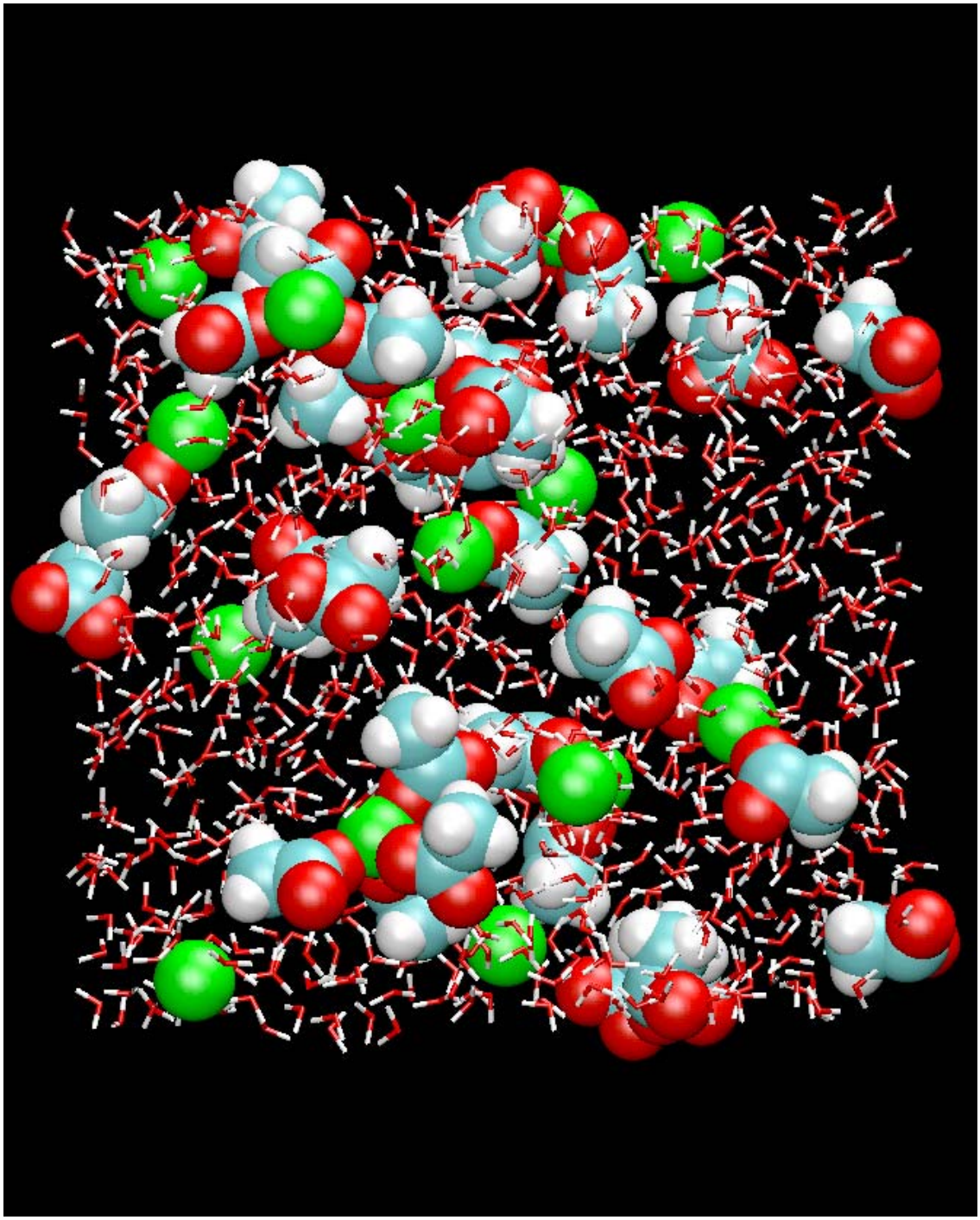

Figure 13. A snapshot from a simulation of 1 M $Mg(OAc)_2$(aq). Color coding: Mg - green, C - cyan, O - red, H - white. For clarity water molecules are displayed in the stick representation.

The qualitative picture from the snapshots was quantified using statistically averaged (over nanosecond trajectories) data. In particular, the Mg^{2+}–anion and ion–water radial distribution functions (RDF) were monitored and cumulative sums

were evaluated as integrals over these RDFs. The cumulative sums were normalized so as to provide the number of anions or water molecules within a particular distance from a Mg^{2+}.

Figure 14 shows the magnesium–nitrate oxygen RDFs and cumulative sums for 0.25 and 1 M solutions. There are no contact ion pairs (which would correspond to a peak in the RDF at around 2.1 Å) present in either case. The RDF peak at 4.2 Å corresponds to ion pairs separated by one water molecule (i. e., a solvent-shared ion pair, SIP). There is also a broad feature at around 6 Å corresponding to ions separated by two water molecules (2SIPs). It can be estimated from the cumulative sum that, on an average, at 0.25 M ≈ 20 % of NO_3^- is transiently associated with Mg^{2+} as SIPs. This rises to about 60 % at 1 M.

a)

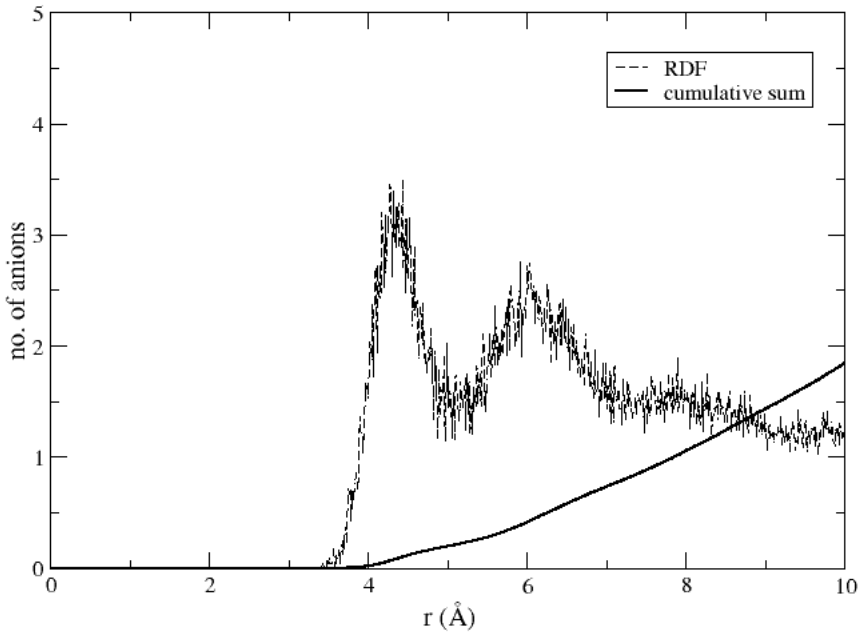

b)

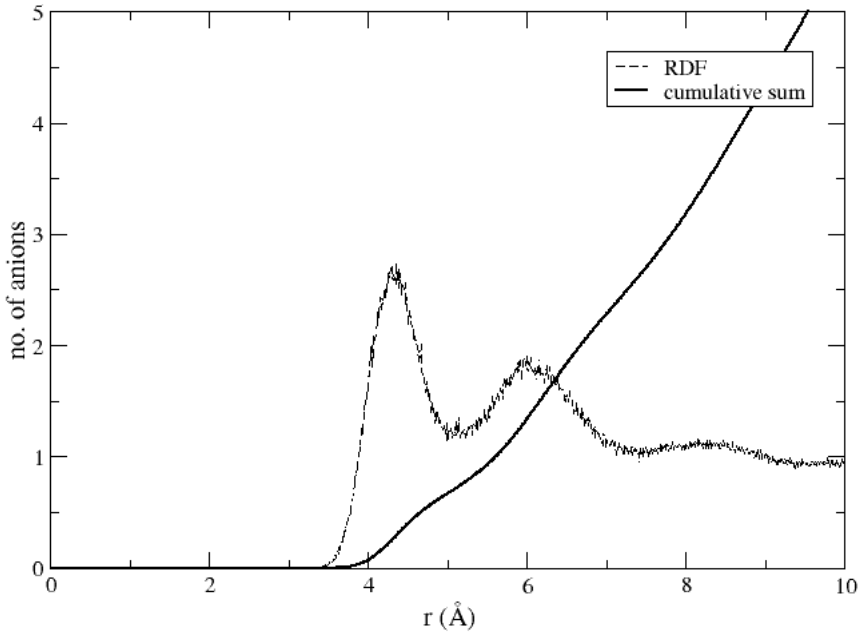

Figure 14. Magnesium–nitrate oxygen radial distribution function and cumulative sum for aqueous solutions at concentrations of: *a*) 0.25 M and *b*) 1 M.

Analogous information for the magnesium acetate solutions is presented in Figure 15. The situation is very different from the nitrate solutions: even at 0.25 M there is significant contact ion pairing, reflected in the RDF peak at around 2.1 Å. From the cumulative sum it can be deduced that ≈ 25 % of Mg^{2+} forms contact ion pairs with OAc^{-}. Moreover, SIPs are also present (at around 4.2 Å). On an average, there is one OAc^{-} per Mg^{2+} present either as CIPs or SIPs. At 1 M this average rises to two, with ≈ 0.7 OAc^{-} per Mg^{2+} present as CIPs.

a)

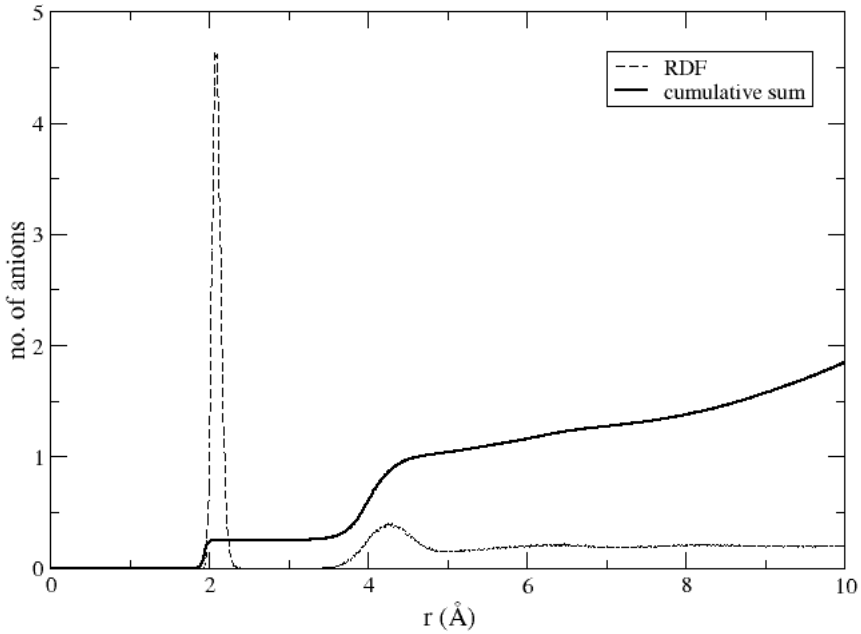

b)

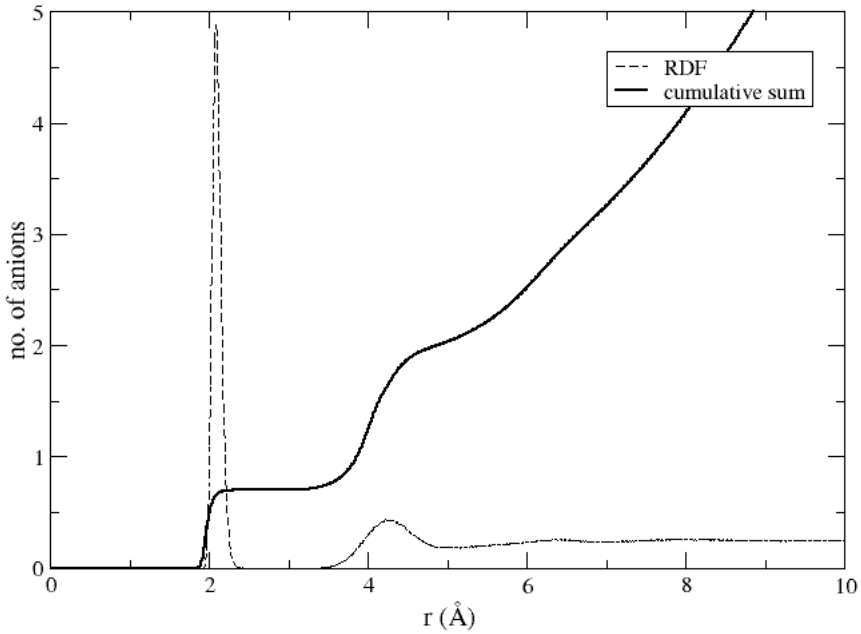

Figure 15. Magnesium–acetate oxygen radial distribution function and cumulative sum for aqueous solutions at a concentration of *a*) 0.25 M and *b*) 1 M.

The ion-water distribution functions provide information about the concentration-dependent hydration patterns of the individual ions. Figure 16 shows the magnesium–water oxygen RDFs and cumulative sum for 0.25 and 1 M solutions of $Mg(NO_3)_2$. For both concentrations there is a rigid first hydration shell around Mg^{2+} containing six strongly bound water molecules, which is typical for alkaline-earth cations. The position of the first hydration shell peak at around 2.1 Å agrees very well with X-ray diffraction experiments.[82] A broader peak at around 4.2 Å marks a much softer second solvation shell containing roughly 12 water molecules. The existence of a second hydration sheath around Mg^{2+} containing 12 water molecules is consistent with both dielectric relaxation measurements[83] and vibrational spectra.[84]

a)

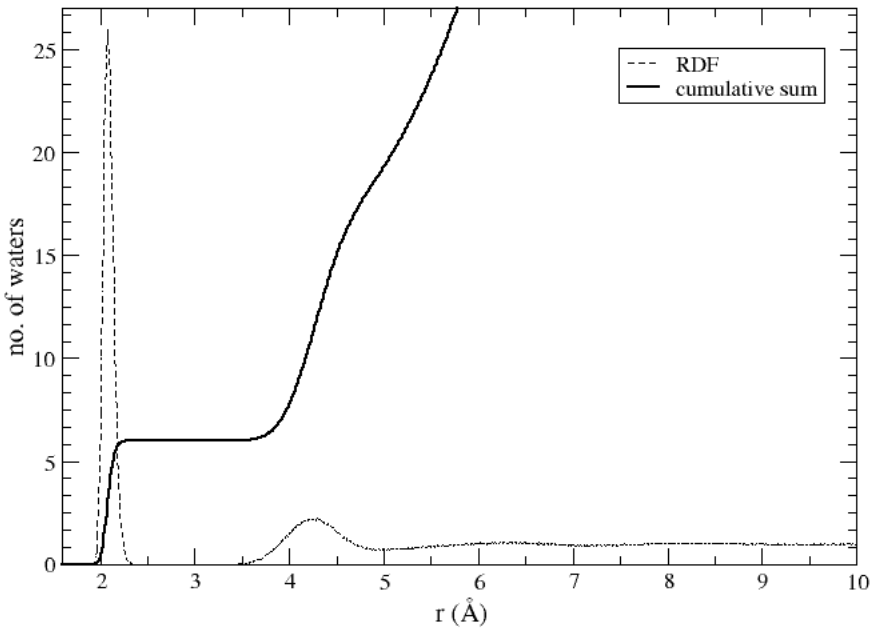

b)

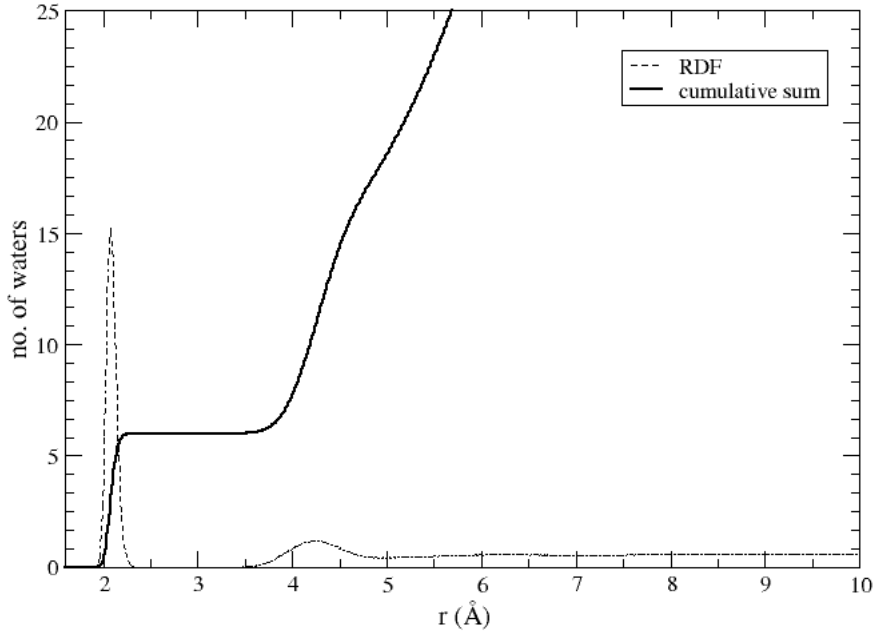

Figure 16. Magnesium–water oxygen radial distribution function and cumulative sum for aqueous solutions of magnesium nitrate at a concentration of *a*) 0.25 M and *b*) 1 M.

The magnesium–water oxygen RDFs and cumulative sums for $Mg(OAc)_2(aq)$, depicted in Figure 17, are affected by strong ion pairing. Thus, the number of water molecules in the first hydration shell drops from 6 to approximately 5.6 at 0.25 M and to 4.8 at 1 M, consistent with them being partially replaced by acetate anions. On an average about one water molecule is displaced from the first hydration shell of Mg^{2+} in 1 M $Mg(OAc)_2$.

a)

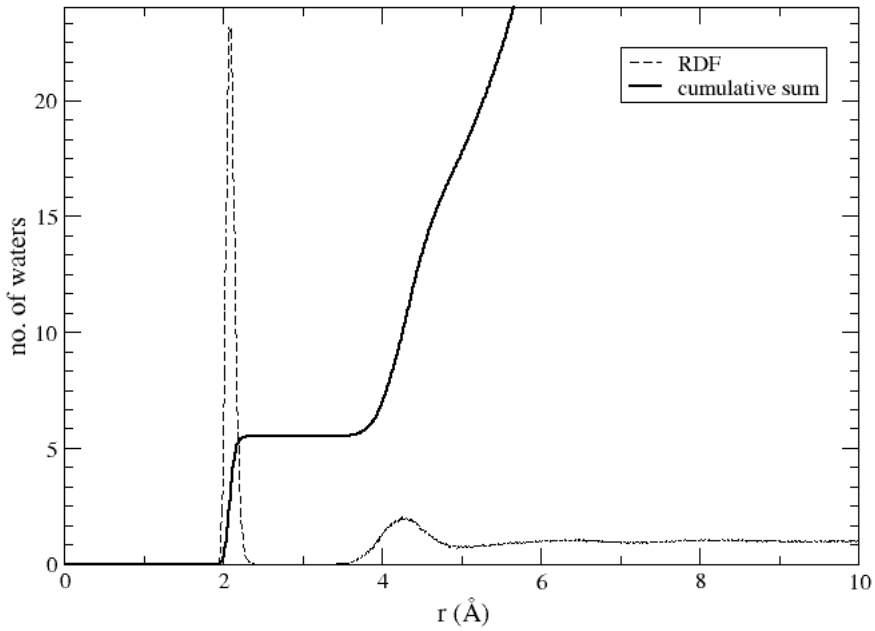
RDF
cumulative sum
no. of waters
r (Å)
0
5
10
15
20
0
2
4
6
8
10

b)

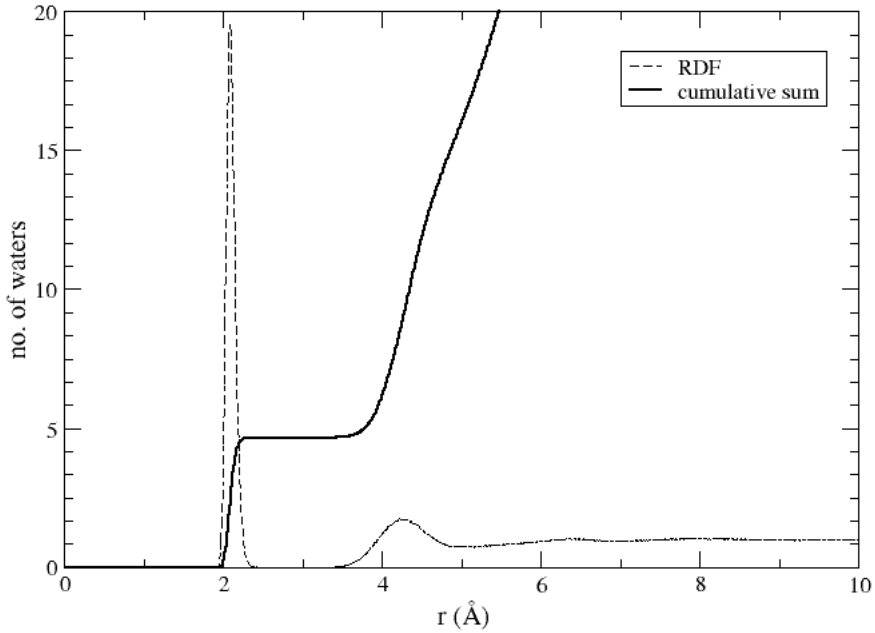
RDF
cumulative sum
no. of waters
r (Å)
0
5
10
15
20
0
2
4
6
8
10

Figure 17. Magnesium–water oxygen radial distribution function and cumulative sum for aqueous solutions of magnesium acetate at a concentration of *a*) 0.25 M and *b*) 1 M.

Test calculations employing polarizable potentials gave very similar results concerning the structure of the solutions and ion pairing as non–polarizable simulations. If anything, the tendency for ion–pairing increased upon inclusion of polarization. This is demonstrated, e.g., in Figure 18, which shows the magnesium–acetate oxygen radial distribution function and cumulative sum for the 0.25 M aqueous solution containing polarizable ions and water molecules. It can be seen that the results compare semiquantitatively to results employing a non-polarizable force field (see Figure 15*a*), except that the direct ion pairing is slightly enhanced.

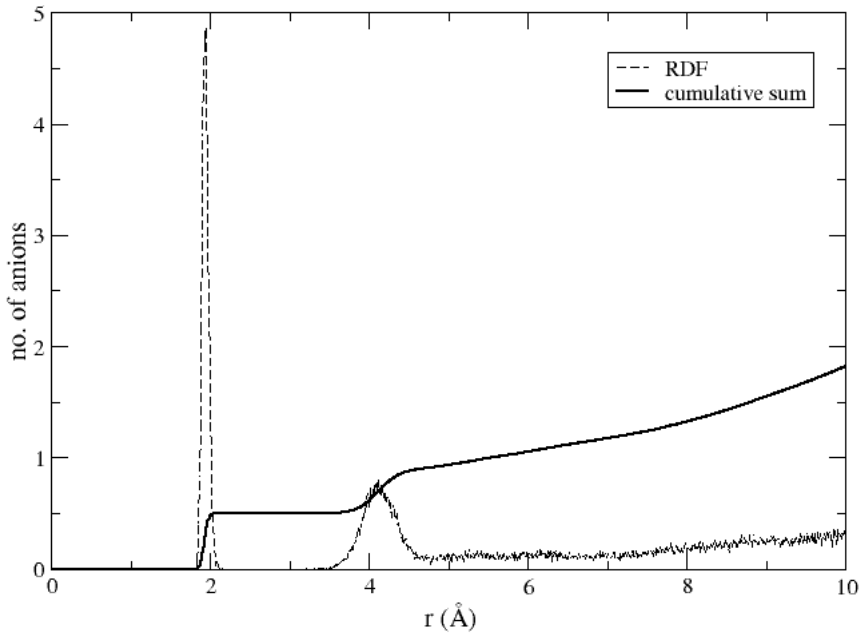

Figure 18. Magnesium–acetate oxygen radial distribution function and cumulative sum for an aqueous solution at a concentration of 0.25 M employing polarizable potentials.

5. Conclusions

Ionic charge density, especially of cations, appears to be a major factor influencing the isentropic compressibilities of aqueous electrolyte solutions. However, the present data for $Mg(OAc)_2$ and $Mg(NO_3)_2$ solutions along with literature values for other salts indicate that anion effects follow the Hofmeister series. The significant differences, which exist between $Mg(OAc)_2$ and $Mg(NO_3)_2$ solutions, with respect to their structural relaxation times, viscosities and electrical conductivities, are consistent with a much greater degree of ion association in the former. This is confirmed by the Raman spectra of $Mg(OAc)_2$(aq), which show substantial changes with concentration, consistent with the formation of mono– and bidentate complexes (contact ion pairs), whereas for $Mg(NO_3)_2$(aq) only non–contact ion pairs are implied. The mean cation–anion separation estimated from a simple geometrical approach suggests that the electrolyte concentration at which $d\kappa_s/dt = 0$, corresponds to the disappearance of "free" solvent from the solution. The experimental results are supported by molecular dynamics simulations of 0.25 and 1 M solutions of magnesium nitrate and acetate. These simulations provide an atomic resolution picture of the ion hydration and pairing in these systems, as well as statistically averaged data. In accord with experiment, contact ion pairs are absent in $Mg(NO_3)_2$ solutions, where only solvent separated ion pairs (SIPs and 2SIPs, the number of which rises steeply with concentration) can be observed. In contrast, contact ion pairs are prevalent in $Mg(OAc)_2$ solutions at both concentrations. The number of CIPs and SIPs increases strongly with concentration and at 1 M a significant ion clustering occurs. This is also reflected in the structure of the first hydration shell around Mg^{2+}, from which on an average about one water molecule is replaced by acetate.

Acknowledgements

Authors (AW and SM) are grateful to the Director, Regional Research Laboratory, Jorhat, India for interest in this work and AW is thankful to the Council of Scientific and Industrial Research, New Delhi, India for the award of senior research fellowship. Support (to PJ) from the Czech Ministry of Education (grant LC512) and from the US-NSF (grants CHE 0431512 and 0209719) is gratefully acknowledged. The authors are also grateful to the Sophisticated Analytical Instrumentation Facility, Indian Institute of Technology-Madras, India for recording the Raman spectra.

References

1. Grossfield, A.; Ren, P.; Ponder, J. W. *J. Am. Chem. Soc.* **2003**, *125*, 15671.
2. Tieleman, D. P.; Biggin, P. C.; Smith, G. R.; Sansom, M. S. P. *Quart. Rev. Biophys.* **2001**, *34*, 473.
3. Hille, B. *Ionic Channels of Excitable Membranes*; 3rd ed., Sinauer Associates Inc.: Sunderland, MA, 2001.
4. Shvartsburg, A. A.; Siu, K. W. M. *J. Am. Chem. Soc.* **2001**, *123*, 10071.
5. Lippard, S. J. *Science* **1993**, *261*, 699.
6. Lide, D. R., Ed.; *Handbook of Chemistry and Physics*; 76th ed., CRC Press: Boca Raton, 1995; p. XIV - 11.
7. Berthelin, J. *Pedologie, Gand* **1982**, *32*, 313.
8. Semmler, J.; Irish, D. E.; Oseki, T. *Geochim. Cosmochim. Acta* **1990**, *54*, 947.
9. Oum, K. W.; Lakin, M. J.; Dehaan, D. O.; Brauers, T.; Finlayson-Pitts, B. J. *Science* **1998**, *279*, 74.
10. Bol, W.; Gerrits, G. J. A.; van Panthaleon van Eck, C. L. *Appl. Cryst.* **1970**, *3*, 486.
11. Bulmer, J. T.; Irish, D. E.; Ödberg, L. *Can. J. Chem*. **1975**, *53*, 3806.
12. Caminiti, R.; Licheri, G.; Piccaluga, G.; Pinna, G. *Chem. Phys. Lett.* **1979**, *61*, 45.
13. Ohtaki, H.; Radnai, T. *Chem. Rev.* **1993**, *93*, 1157.
14. Markham, G. D.; Glusker, J. P.; Bock, C. L.; Trachtman, M.; Bock, C.W. *J.Phys. Chem.* **1996**, *100*, 3488.
15. Pavlov, M. P.; Siegbahn, E. M.; Sandström, M. *J. Phys. Chem. A* **1998**, *102*, 219.
16. Pye, C. C.; Rudolph, W. W. *J. Phys. Chem. A* **1998**, *102*, 9933.
17. Righellato, E. C.; Davies, C. W. *Trans. Faraday Soc.* **1930**, *26*, 592,
18. Robinson, R. A.; Wilson, J. M.; Ayling, H. S. *J. Am. Chem. Soc.* **1942**, *64*, 1469.
19. Vollmar, P. M. *J. Chem. Phys.* **1963**, *39*, 2236.
20. Irish, D. E.; Chang, T. G.; Nelson, D. L. *Inorg. Chem.* **1970**, *9*, 425.
21. Peleg, M. *J. Phys. Chem.* **1972**, *76*, 1019.
22. Chang, T. G.; Irish, D. E. *J. Phys. Chem.* **1973**, *77*, 52.
23. Zhang, Y.-H.; Choi, M. Y.; Chan, C. K. *J. Phys. Chem. A* **2004**, *108*, 1712.
24. James, D. W.; Carrick, M. T.; Frost. R. L. *J. Raman Spectrosc.* **1982**, *13*, 115.

25. Tomišić, V.; Simeon, V. *Phys. Chem. Chem. Phys.* **2000**, *2*, 1943.
26. James, D. W.; Frost, R. L. *Aust. J. Chem.* **1982**, *35*, 1793.
27. Angell, C. A.; *J. Electrchem. Soc.* **1965**, *112*, 1224.
28. Irish, D. E.; Nelson, D. L.; Brooker, M. H.; *J. Chem. Phys.* **1971**, *54*, 654.
29. Caminiti, R.; Cucca, P.; Monduzzi, M.; Saba, G.; Crisponi, G. *J. Chem. Phys.* **1984**, *81*, 543.
30. Shehata, H. A. *J. Chem. Soc. Faraday Trans.* **1994**, *90*, 3401.
31. Purdie, P.; Barlow, A. J. *J. Chem. Soc. Faraday Trans. II* **1972**, *68*, 33.
32. Tackett, J. E. *Appl. Spectrosc.* **1989**, *43*, 483.
33. Nickolov, Zh.; Ivanov, I.; Georgiev, G.; Stoilova, D. *J. Mol. Struct.* **1996**, *377*, 13.
34. Quilès, F.; Burneau, A. *Vibrational Spectrosc.* **1998**, *16*, 105.
35. Wang, L.-Y.; Zhang, Y.-H.; Zhao, L.-J. *J. Phys. Chem. A* **2005**, *109*, 609.
36. Hofmeister, F. *Naum-Schmiedebergs Archiv Expt. Pathol. Pharmakol.* **1888**, *23*, 247. English translation: Kunz, W.; Henle, J.; Ninham, B. W. *Curr. Opin. Colloid Interface Sci*. **2004**, *9*, 19.
37. (a) Cacace, M. G.; Landau, E. M.; Ramsden, J. J. *Quart. Rev. Biophys*. **1997**, *30*, 241. (b) Kunz, W.; Lo Nostro, P.; Ninham, B. W, *Curr. Opin. Colloid Interface Sci.* **2004**, *9*, vii.
38. Kunz, W.; Lo Nostro, P.; Ninham, B. W. *Curr. Opin. Colloid Interface Sci.* **2004**, *9*, 1.
39. Vogel, A. I. *Textbook of Quantitative Inorganic Analysis*; 4th ed.; ELBS; Longman: U.K., 1985, p. 316.
40. Wahab, A.; Mahiuddin, S. *J. Chem. Eng. Data* **2004**, *49*, 126.
41. Rohman, N.; Wahab, A.; Mahiuddin, S. *J. Solution Chem.* **2005**, *34*, 77.
42. Rohman, N.; Dass, N. N.; Mahiuddin, S. *J. Chem. Eng. Data* **1999**, *44*, 465.
43. Allen, M. P.; Tildesley, D. J. *Computer Simulatons of Liquids*, Clarendon, Oxford, 1987.
44. Essmann, U.; Perera, L.; Berkowitz, M. L.; Darden, T.; Lee, H.; Pedersen, L. G. *J. Chem. Phys*. **1995**, 103, 8577.
45. Ryckaert, J.-P.; Ciccotti, G.; Berendsen, H. J. C. *J. Comp. Phys*. **1977**, 23, 327.
46. Thole, B. T. *Chem. Phys*. **1981**, 59, 341.

47. Vrbka, L.; Mucha, M.; Minofar, B.; Jungwirth, P.; Brown, E. C.; Tobias, D. J. *Curr. Opin. Colloid Interface Sci*. **2004**, 9, 67.
48. Berendsen, H. J. C.; Grigera, J. R.; Straatsma, T. P. *J. Phys. Chem*. **1987**, 91, 6269.
49. Wang, J. M.; Wolf, R. M.; Caldwell, J. M.; Kollman, P. A. *J. Comp. Chem*. **2004**, 25, 1157.
50. Jorgensen, W. L. *OPLS and OPLS-AA Parameters for Organic Molecules, Ions, and Nucleic Acids*, Yale University, 1997.
51. Frisch, M. J.; Trucks, G. W.; Schlegel, H. B.; Scuseria, G. E.; Robb, M. A.; Cheeseman, J. R.; Montgomery, Jr., J. A.; Vreven, T.; Kudin, K. N.; Burant, J. C.; Millam, J. M.; Iyengar, S. S.; Tomasi, J.; Barone, V.; Mennucci, B.; Cossi, M.; Scalmani, G.; Rega, N.; Petersson, G. A.; Nakatsuji, H.; Hada, M.; Ehara, M.; Toyota, K.; Fukuda, R.; Hasegawa, J.; Ishida, M.; Nakajima, T.; Honda, Y.; Kitao, O.; Nakai, H.; Klene, M.; Li, X.; Knox, J. E.; Hratchian, H. P.; Cross, J. B.; Bakken, V.; Adamo, C.; Jaramillo, J.; Gomperts, R.; Stratmann, R. E.; Yazyev, O.; Austin, A. J.; Cammi, R.; Pomelli, C.; Ochterski, J. W.; Ayala, P. Y.; Morokuma, K.; Voth, G. A.; Salvador, P.; Dannenberg, J. J.; Zakrzewski, V. G.; Dapprich, S.; Daniels, A. D.; Strain, M. C.; Farkas, O.; Malick, D. K.; Rabuck, A. D.; Raghavachari, K.; Foresman, J. B.; Ortiz, J. V.; Cui, Q.; Baboul, A. G.; Clifford, S.; Cioslowski, J.; Stefanov, B. B.; Liu, G.; Liashenko, A.; Piskorz, P.; Komaromi, I.; Martin, R. L.; Fox, D. J.; Keith, T.; Al-Laham, M. A.; Peng, C. Y.; Nanayakkara, A.; Challacombe, M.; Gill, P. M. W.; Johnson, B.; Chen, W.; Wong, M. W.; Gonzalez, C.; and Pople, J. A. *Gaussian 03*, Gaussian, Inc., Wallingford CT, 2004.
52. Case, D. A.; Darden, T. A.; Cheatham, III, T. E.; Simmerling, C. L.; Wang, J.; Duke, R. E.; Luo, R.; Merz, K. M.; Wang, B.; Pearlman, D. A.; Crowley, M.; Brozell, S.; Tsui, V.; Gohlke, H.; Mongan, J.; Hornak, V.; Cui, G.; Beroza, P.; Schafmeister, C.; Caldwell, J. W.; Ross, W. S.; Kollman, P.A. *AMBER 8*, University of California, San Francisco, 2004.
53. Caldwell, J.; Kollman, P. A. *J. Phys. Chem.* **1995**, *99*, 6208.
54. Wang, J. M.; Cieplak, P.; Kollman, P. A. *J. Comp. Chem*. **2000**, *21*, 1049.
55. Petersen, P. B.; Mucha, M.; Jungwirth, P.; Saykally, R. J., *J. Phys. Chem. B* **2005**, *109*, 10915.

56. Emara, M. M.; Farid, N. A. *J. Indian Chem. Soc.* **1981**, 58, 474.
57. Doan, T. H.; Sangster, J. *J. Chem. Eng. Data* **1981**, *26*, 141.
58. Mahiuddin, S.; Ismail, K. *Can. J. Chem*. **1982**, *60*, 2883.
59. Behrends, R.; Miecznik, P.; Kaatze, U. *J. Phys. Chem. A* **2002**, *106*, 6039.
60. Phillips, C. G.; Williams, R. J. P. *Inorganic Chemistry*; Clarendon Press: New York, 1965, Vol. 1, p. 161.
61. Marcus, Y.; Hefter, G. *Chem. Rev*. **2004**, *104*, 3405.
62. Marcus, Y. *Ion Solvation*; John Wiley & Sons: Chichester, U.K., 1985, ch. 3.
63. Ohtaki, H. *Monatsh. Chem.* **2001**, *132*, 1237.
64. Millero, F. J.; Ricco, J.; Schreiber, D. R. *J. Solution Chem.* **1982**, *11*, 671.
65. Marcus, Y. *Ion Properties*; Marcel Dekker: New York, 1997.
66. Rohman, N.; Mahiuddin, S. *J. Chem. Soc. Faraday Trans.* **1997**, *93*, 2053.
67. Rohman, N.; Dass, N. N.; Mahiuddin, S. *J. Mol. Liquids* **2002**, *100/3*, 265.
68. Gurney, R. W. *Ionic Processes in Solutions*; Dover Publications: New York, 1953.
69. *International Critical Tables of Numerical Data, Physics, Chemistry and Technology*; Washburn, E. W. (Ed.), McGraw-Hill: New York, **1928**; (a) Vol. VI, p. 254; (b) Vol. VI, p. 238.
70. Harned, H. S.; Owen, B. B. *The Physical Chemistry of Electrolytic Solutions*; 2nd ed., Reinhold Publishing Corporation: New York, 1950, p. 172.
71. Koga, Y.; Westh, P.; Davies, J. V.; Miki, K.; Nishikawa, K.; Katayanagi, H. *J. Phys. Chem. A* **2004**, *108*, 8533.
72. Waterland, M. R.; Stockwell, D.; Kelley, A. M. *J. Chem. Phys.* **2001**, *114*, 6249.
73. Nancollas, G. H. *J. Chem. Soc*. **1956**, 744.
74. Frost, R. L.; Kloprogge, J. T. *J. Mol. Struct.* **2000**, *526*, 131.
75. Padmanabhan, A. C.; Srinivasan, R. *Indian J. Pure Appl. Phys.* **1973**, *11*, 404.
76. Hester, R. E.; Plane, R. A. *Spectrochim. Acta* **1967**, *23A*, 2289.
77. Bickley, R. I.; Edwards, H. G. M.; Rose, S. J.; Guster, R. *J. Mol. Struct.* **1990**, *238*, 15.
78. Irish, D. E.; Davis, A. R. *Can. J. Chem.* **1968**, *46*, 943.
79. Zhang, Y.-H.; Chan, C. K. *J. Phys. Chem. A* **2003**, *107*, 5956.
80. Walrafen, G. E. *J. Chem. Phys.* **1962**, *36*, 1035.

81. For example, a one molar $Mg(OAc)_2$ solution is considered where the water molecules are taken as hard spheres of radius 1.4 Å. The ionic radius of Mg^{2+} and OAc^- is taken as 0.65 and 2.32 Å and the corresponding volume would be 1.15 and 52.31 $Å^3$, respectively. At this concentration, ions would constitute a volume fraction of 6.37%. Now, a spherical box is taken to fill it randomly with the particles (ions) so that 6.37% is occupied. The maximum possible mean distance between a cation and an anion along the diameter of the sphere is calculated to be 11.72 Å.
82. Marcus, Y. *Chem. Rev*. **1988**, *88*, 1475.
83. Buchner, R.; Chen, T.; Hefter**,** G. T. *J. Phys. Chem. B*, **2004**, *108*, 2365.
84. Rudolph, W. W.; Irmer, G.; Hefter, G. T. *Phys. Chem. Chem. Phys.* **2003**, *5***,** 5253.